Atomistic Simulation of a Glassy Polymer Surface

Kevin F. Mansfield and Doros N. Theodorou*

Department of Chemical Engineering, University of California, Berkeley, and Center for Advanced Materials, Lawrence Berkeley Laboratory, Berkeley, California 94720

Received November 13, 1989; Revised Manuscript Received March 21, 1990

ABSTRACT: An atomistically detailed computer simulation of a glassy atactic polypropylene surface exposed to vacuum has been performed. Local structural features and interfacial thermodynamic properties have been calculated by averaging over sets of static model microstates. Each microstate was obtained by Monte Carlo generation, followed by total potential energy minimization. The internal energy contribution to surface tension, predicted from interatomic forces and distances on the basis of a new formulation, based on dilating the surface area, is within 7% of the experimental value. The density profile in the interfacial region is sigmoidal. Backbone bonds exhibit a tendency to orient parallel to the surface. The distribution of rotational states of skeletal bonds is perturbed relative to the bulk. All the above structural features are observed within a 10-Å-thick region at the vacuum/polymer interface. At the level of entire chains, structure deviates from its bulk characteristics over a region of thickness commensurate with overall chain dimensions. The distribution of chain centers of mass displays a maximum roughly one radius of gyration away from the edge of the polymer. The average chain width parallel to the surface is significantly larger near the edge of the polymer than in the bulk. This is because chains in the interfacial region display a tendency to orient with their longest span and their longest principal axis parallel to the surface. The dependence of structural features on polymer molecular weight is discussed.

1. Introduction

The surface properties of polymers, in the condensed amorphous state, play a very significant role in shaping the overall performance of many materials systems. The role of polymers is becoming increasingly important in manufacturing surfaces with controlled friction and wear characteristics and in manipulating wettability by aqueous and organic fluids. Establishing quantitative relations between chemical constitution and macroscopically manifested surface properties would constitute an important step toward the rational design of multiphase materials containing polymers.

Statistical mechanics based computer simulation can be used to reliably predict macroscopic properties from molecular-level information. In addition, computer simulation is an excellent tool for exploring local structure and properties in the interfacial region, especially since experimental evidence on macromolecular organization at the surfaces of condensed, solvent-free polymers is scarce.

Recently, there has been considerable interest in simulating the free surface of dense, multichain polymer systems. A lattice Monte Carlo simulation of the free surface of a polymer melt was presented by Madden,[1] using an efficient pseudokinetic algorithm. The method has recently been extended to the continuum, using freely jointed chains of loosely bonded beads.[2] Furthermore, there has been much interest in simulating polymer melts between solid surfaces. Lattice Monte Carlo simulations in this geometry were presented by ten Brinke et al.[3] and Mansfield and Theodorou.[4] Off-lattice Monte Carlo simulations have been performed by Kumar et al.[5] and by Yethiraj and Hall.[6] A molecular dynamics simulation has also been applied by Bitsanis and Hadziioannou[7] to study bead-and-spring polymeric liquids between solid walls.

The work reported in this paper concerns the free surface of a *glassy* polymer. Unlike previous simulations, it aims at quantitatively predicting interfacial thermodynamic properties, in addition to elucidating microscopic surface structure. A detailed atomistic model is employed, in which molecular geometry and energetics are represented with a high degree of realism. Our approach, much more elaborate in many ways than those used in other investigations, has been designed so as to allow direct comparison against experiment. The molecular representation and simulation methodology developed here come as an extension of previous work on bulk glassy polymers,[8-11] which proved remarkably successful in predicting properties such as cohesive energy density, elastic constants, and X-ray diffraction patterns. The generality of our molecular picture of the glassy state is put to test under the highly anisotropic conditions prevailing at the surface.

Glassy polymers are not in a state of thermodynamic equilibrium. Nevertheless, in many applications they can be adequately treated as ordinary solids. At the microscopic level they can be viewed as assemblages of disordered microstructures, which are "locked" in the vicinity of local minima of potential energy in configuration space. The passage from one such minimum to neighboring minima (relaxation), which occurs readily by chain self-diffusion in the liquid state, is very slow in glasses. Thermal motion consists mainly of localized segmental fluctuations within the potential energy wells, in which the glassy structure is locked. Consistent with this picture, we have developed a simulation approach in which a well-relaxed glassy polymer film is represented as a set of static microstates, each in detailed mechanical equilibrium (Appendix A). The microstates are created in such a manner that the average density in their bulk region (middle of the film) equals the experimental density of the glassy polymer under given conditions of temperature ($T > 0$ K) and ambient pressure ($P \rightarrow 0$). It is through the bulk density that we assign a temperature to these static simulations.

Each microstate constitutes a local minimum of total potential energy with respect to all configurational degrees of freedom under the considered bulk density. This minimum is designed to represent the structure around which a small region of the real polymer glass would fluctuate at the temperature and pressure considered. Our microstates do not comprise a statistical mechanical ensemble; it is not implied that, given sufficient time, a

* To whom correspondence should be addressed at the University of California.

0024-9297/90/2223-4430$02.50/0

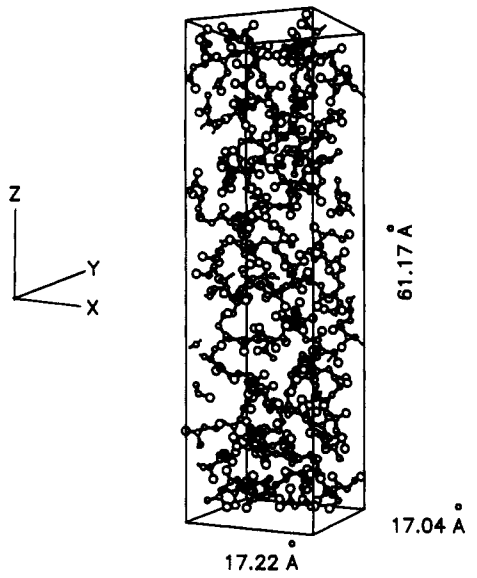

Figure 1. "Relaxed" model structure of a thin film of polymer composed of several $H-[CH_2-(CH_3)]_{76}-CH_3$ chains exposed to vacuum at its upper and lower surfaces. The smaller and larger spheres correspond to carbons and methyls, respectively. The temperature and bulk density were chosen so as to simulate the polymer in its glassy state.

given region of the polymer would sample all these microstates with a certain probability distribution. Rather, we assert that, if an atomic-scale observer were to take a walk through an actual amorphous solid polymer film, he would encounter a variety of regions, each of which would resemble (fluctuate around) one of the microstates we generate.

Structural, thermodynamic, and mechanical properties of the polymer film are estimated by arithmetically averaging the properties of individual static microstates. Again, this operation corresponds to a spatial averaging over small regions throughout an amorphous solid macroscopic system, rather than to an ensemble averaging; this is why all microstates are attributed the same weight.

The microscopic model we developed to study the surface of a glassy polymer, atactic polypropylene, is described in section 2 of this paper. Our simulation methodology is outlined in section 3. Results on microscopic structure and our prediction for a thermodynamic property, the internal energy contribution to surface tension, are presented in section 4. Finally, our findings are summarized in section 5. Conceptual and mathematical details of the formulation are elaborated in the appendices.

2. The Model

The system we examine in this work is a very thin film of glassy atactic polypropylene exposed to vacuum on both sides. A model microstate representing this film is shown in Figure 1. It is created within an orthorhombic box, or "unit cell", of dimensions $h_1 = 17.22$ Å, $h_2 = 17.04$ Å, and $h_3 = 61.17$ Å in the x, y, and z directions, respectively, and it is filled with segments from several polymer chains. Periodic boundary conditions[12] are implemented in the x and y directions only; they permit treating the box as part of a system that is macroscopic in these two directions. The resulting geometry is that of a 61.17-Å-thick polymer film of effectively infinite extent, having two well-defined surfaces located at the upper and lower extremes of the cell, perpendicular to the z axis. The film thickness was chosen large enough to make the middle region indistinguishable from bulk polymer, yet small enought to keep computations tractable. Recent modeling and simulation work on polymer melt surfaces[1,2,13] indicates that the anisotropy in local structural features does not extend beyond two radii of gyration away from each surface. In view of this, and given that the top and bottom surfaces of our film are separated by roughly 3.5 times the unperturbed radius of gyration, they should behave independently of each other, to a good approximation. Evidence for this will be presented in section 4.

Equilibrium atactic polypropylene was chosen as the polymer because of its noncrystallizable stereochemistry and simple chemical constitution; the interatomic interaction potentials and conformation statistics are relatively well-known for this polymer. Also, the choice of atactic polypropylene facilitates comparison against previous bulk results.[8-10] Our model polymer is monodisperse, consisting of linear chains of the form $RCHR(CH_2CHR)_{x-1}R$, where R is a methyl group. The degree of polymerization is $x = 76$ and corresponds to a molecular weight of 3214. The chain tacticity is Bernoullian with a fraction of meso diads $w_m = 0.48$, as is experimentally observed in equilibrium-epimerized polypropylene. Each unit cell is constructed out of three "parent" chains, yielding a bulk density of 0.892 g/cm^3. This corresponds to the experimental density of atactic polypropylene at −40 °C (roughly 20 °C below the glass transition temperature), which is the temperature we wish to model. Our force field representation follows previous work.[8,14] Bond angles and lengths are fixed, and methyl groups are treated as single "quasi-atoms". Conformational rearrangement can occur through torsion around skeletal bonds. van der Waals interactions between all pairs of atomic species present are described by truncated Lennard-Jones potentials, made continuous by substituting the potential tail by a quintic spline. The potential parameterization is identical with that used in our earlier work.[8]

3. The Simulation

The basic assumptions underlying our simulation are summarized in the Introduction and in Appendix A. The film is viewed as glassy over its entire thickness. Our method calls for creating a set of static microstates, representative of possible local configurations of the actual film, and subsequently averaging their properties arithmetrically. The creation of a model microstate is accomplished in two steps. First, an initial-guess structure is generated. Second, the initial-guess structure is converted into one satisfying the requirements of detailed mechanical equilibrium by minimizing its total potential energy with respect to all microscopic degrees of freedom. The second step, energy minimization, is by far the most demanding computationally. Its central processing unit (CPU) requirements can be significantly reduced by choosing a realistic initial guess. Therefore, considerable efforts were devoted to enhancing the performance of the initial guess part of the simulation.

The initial-guess problem entails the generation of a liquidlike multichain configuration which is consistent with short-range intramolecular energetics, free of excessive long-range atom–atom overlaps (repulsions due to excluded volume), and situated between two vacuum phases. The stereochemical configuration of the three parent chains is specified first. This is done by Monte Carlo generation of three Bernoullian sequences of meso and racemic diads, each containing 48% meso diads. Next, the locations (chain start coordinates) and orientations (Eulerian angles) of the first two skeletal bonds of each chain are randomly assigned inside the unit cell. Subsequently, the con-

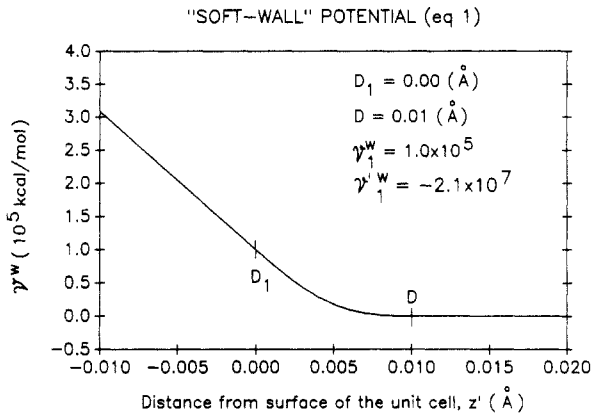

Figure 2. "Soft-wall" potential used in the initial-guess and preliminary stages of the total potential energy minimization. Such a wall is placed at the upper and lower bounds of the z axis, normal to the xy plane.

formations (sequences of torsion angles) are chosen by "growing" the chains simultaneously in a bond-by-bond fashion within the unit cell. As in our previous work, a discrete representation of conformations is used, based on a five-state rotational isomeric state model (RIS) of polypropylene.[15] Two-dimensional periodic boundary conditions are observed during this procedure of growing conformations. In the course of this initial-guess generation, it is important to prevent chains from exiting the film and wandering into the surrounding vacuum. This is accomplished by placing "soft walls" at the upper and lower faces of the unit cell. At each face, the soft wall consists of a steeply repulsive, smooth, ramplike potential experienced by the chain atoms:

$$\mathcal{V}^w(z') = \begin{cases} \mathcal{V}_1'^w z' + \mathcal{V}_1^w & z' < D_1 \quad (1a) \\ (1-\xi)^3[\mathcal{V}_1^w + (3\mathcal{V}_1^w + \mathcal{V}_1'^w\Delta)\xi + (6\mathcal{V}_1^w + 3\mathcal{V}_1'^w\Delta)\xi^2] & D_1 \le z' < D \quad (1b) \\ 0 & z' \ge D \quad (1c) \end{cases}$$

$\mathcal{V}^w(z')$ is depicted in Figure 2. z' is the distance of an atom from the surface face of the unit cell (z' assumes negative values when the considered atom lies outside the unit cell); $\mathcal{V}_1^w$ and $\mathcal{V}_1'^w$ are the value and first derivative of the wall potential at the junction point $z' = D_1$; $\Delta = (D - D_1)$; and $\xi = (z' - D_1)/(D - D_1)$. $\mathcal{V}_1'^w$ and $\mathcal{V}_1^w$ are related by

$$\mathcal{V}_1'^w = -25\mathcal{V}_1^w/12\Delta \quad (2)$$

With this choice, the curvature of the wall potential is nonnegative over the entire range of its definition. All initial-guess generations were carried out with $D_1 = 0$, $D = 0.01$ Å, and $\mathcal{V}_1^w = 1 \times 10^5$ kcal/mol. The same wall potential was applied to all types of atoms.

The presence of steep walls necessitated improvements in the Monte Carlo conformation generation algorithm over that used in our previous work.[8] We designed a new, two-bond equivalent Markov scheme for the surface simulations. In order to decide on the conformation of bond i of a parent chain, this new scheme first evaluates conditional RIS probabilities $q_{\xi\eta;i,i+1}$, for all possible combinations of states (ξ,η) of bonds i and $i+1$, given the state ζ of bond $i-1$. These probabilities are calculated from the statistical weight matrices used in the RIS description of the conformational partition function of an unperturbed chain.[16,17] Modified conditional probabilities for all possible states ξ of bond i are then formed, taking into account all long-range intersegmental as well as segment/wall interactions introduced by chain atoms associated with bonds i and $i+1$ (see Appendix B). This two-bond scheme allows a chain ample freedom to redirect itself in the presence of an approaching wall or in anticipation of a severe excluded volume overlap. Unlike the old one-bond algorithm, the new algorithm is always successful in the presence of confining walls and leads to initial-guess energies that are typically lower by an order of magnitude.

The initial-guess structure is converted to a microstructure satisfying the conditions of detailed mechanical equilibrium via potential energy minimization. Physically, the model chains are allowed to change their orientations and conformations through changes in their Eulerian and bond torsion angles; they are also allowed to change their location with respect to each other and to the vacuum phases through translations along the three coordinates. The total potential energy of one of our model structures, exposed to vacuum on both sides, can be expressed as a function of $N_c(2x + 4) - 3 = 465$ microscopic degrees of freedom where $N_c = 3$ chains. These are the start coordinates of the second and third chain relative to the first one ($x_{0,i} - x_{0,1}$, $y_{0,i} - y_{0,1}$, $z_{0,i} - z_{0,1}$, where $i = 2, 3$); a total of nine Eulerian angles, three per chain, specifying the overall orientation of the parent chains with respect to the unit cell frame of reference ($\psi_{1,i}$, $\psi_{2,i}$, $\psi_{3,i}$, where $i = 1, 2, 3$); and the sequence of $2x - 2 = 150$ torsion angles for all rotatable skeletal bonds of each chain ($\phi_{2,i}$, $\phi_{3,i}$, ..., $\phi_{151,i}$, where $i = 1, 2, 3$). The total potential energy minimization is performed by using the quasi-Newton matrix updating algorithm of Broyden, Fletcher, Goldfarb, and Shanno.[18] Analytically calculated first derivatives are implemented (Appendix C). As in previous work,[8] the energy is minimized by a three-stage optimization strategy, which invokes successively the following potential representations: (i) "soft-sphere", purely repulsive interatomic interaction potential, with van der Waals radii reduced to half their actual size and no rotational barriers; (ii) "soft-sphere" potential with actual radii and full rotational barriers; (iii) full potential, including attractive interatomic interactions. During both "soft-sphere" potential stages, the repulsive "soft walls" (eq 1) are retained at the nonperiodic boundaries to prevent the polymer from coming apart under the influence of repulsive interactions. Notice that this necessitates including the start coordinate $z_{0,1}$ of the first chain as an additional degree of freedom during stages i and ii. In the minimization, the wall potential parameters are slightly different from those employed in the initial-guess generation. While D_1 and D are retained at 0 and 0.01 Å, respectively, $\mathcal{V}_1^w$ is lowered to 1×10^2 kcal/mol. Also the wall potential is applied only to backbone carbon atoms. These changes allow the polymer more rotational freedom at the interface, thus minimizing the artificial effect of the wall on polymer conformation. During stage iii the walls are completely removed, and the polymer is allowed to relax solely under the influence of its own cohesive interactions. The density is no longer constrained anywhere in the cell: the model film may expand or contract while driving itself into a local minimum of potential energy. Typically, the density in the middle region of the final relaxed structure is very close to the initially preset (bulk) density (see section 4). The two resulting free surfaces exhibit some degree of "waviness" at the molecular level.

All computations were performed on the Cray X-MP/48 at the San Diego Supercomputer Center; programs were written in FORTRAN. The energy minimization code was extensively optimized for maximal efficiency. Code enhancements include the use of the "conditional vector merge" function,[19] which makes it possible to find the

Table I
Central Processing Unit (CPU) Time Requirements for Obtaining a Model Microstate[a]

stage	no. of function evaluations	CPU time, min
initial guess		2
i	300 ± 60	2 ± 1
ii	9410 ± 1390	33 ± 6
iii	1900 ± 390	67 ± 16

[a] Degree of polymerization $x = 76$. Figures represent averages over 20 cases. FORTRAN computations performed on a Cray X-MP/48, located at San Diego Supercomputer Center, and compiled under CFT77 3.0.

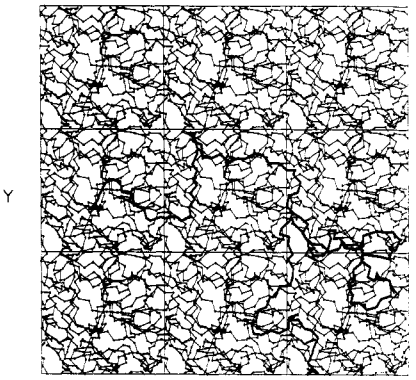

Figure 3. xy projection of nine adjacent images of a model microstate. A single parent chain is highlighted.

squared minimum image distances between all atom pairs in a vectorized manner; and the implementation of a Verlet neighbor list,[12] with a skin thickness of 0.2 times the Lennard-Jones collision diameter for all atom pairs. A breakdown of CPU time requirements for obtaining a typical structure appears in Table I.

To assess system size effects as well as the relation between surface structure and polymer molecular weight, a series of simulations were performed on a shorter chain system. In these simulations, nine polypropylene parent chains of tacticity $w_m = 0.50$ and degree of polymerization $x = 25$ (50 skeletal bonds, molecular weight of 1068) were used in place of the three parent chains of the base case ($x = 76$) simulations. The unit cell dimensions were the same, and the initial-guess generation and potential energy minimization proceeded in the same manner as previously described. The resulting microstates corresponded to a glassy film of short chains with approximately the same bulk density and temperature as the base case simulations. A total of 20 low molecular weight microstates were generated for comparison with the base case results.

4. Results

Structure. Our computer-generated static microstates provide detailed information on molecular organization, both at the scale of individual segments and at the scale of entire chains. More importantly, they allow the prediction of surface thermodynamic properties. Results presented herein refer to the $x = 76$ system, unless otherwise indicated. They constitute arithmetic averages over 70 relaxed microstates, each representing a probable local configuration of a thin glassy polymer slab (Appendix A). The microstates are remarkably close in energy; the standard deviation of the total potential energy is only 0.05 kT/atom. Shown in Figure 3 is an xy projection of a single unit cell, surrounded by eight replicas of itself; the role played by two-dimensional periodic boundary conditions is evident. Three adjacent zx projections are portrayed

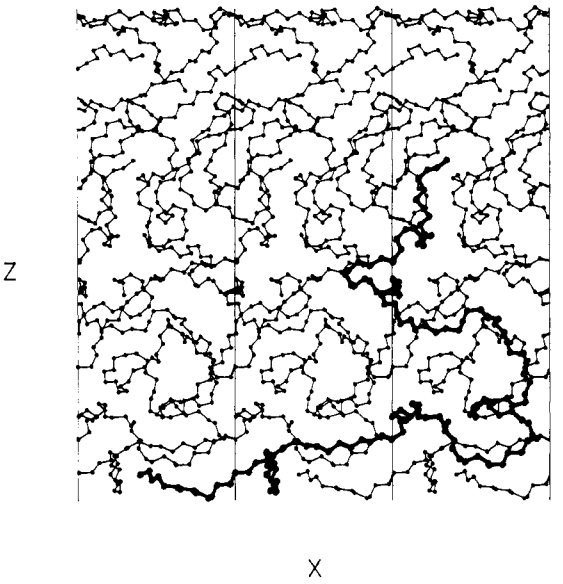

Figure 4. Three adjacent zx projections of the same model structure, with the same single parent chain highlighted as in Figure 3. The zx projection looks less dense than the xy projection of Figure 3 simply because the unit cell is thicker in the z direction.

in Figure 4; the location of the two polymer/vacuum interfaces is clearly displayed. In both Figures 3 and 4, one of the three parent chains is traced with a bold line. Some flattening in the shape of the chain is evident as it approaches the free surface.

In the course of the energy minimization, a model film may drift slightly relative to the initial boundaries of the unit cell. To evaluate average structural features, we superpose all minimum-energy microstates so that the z coordinates of their centers of mass coincide. The z dependence of structural characteristics is thus examined at a very local level. Any fluctuations in structure occurring over wavelengths larger than 17.04 Å in transverse directions (x, y) are cut off. The superposed model films are partitioned into equal bins by drawing planes normal to the z axis, and the contents of each bin are analyzed. Moreover, since the two faces of the film are macroscopically symmetric, each microstate is superposed with its mirror image with respect to its midplane. Thus, our results represent averages over 140 half-structures, accumulated within each bin. In the following, all structural features are displayed as functions of distance z over half the film only. Position $z = 0$ corresponds to the film midplane, and vacuum lies at large z values.

The local mass density distribution, accumulated using 1-Å-thick bins along the z axis, is displayed in Figure 5. Error bars in this and all subsequent plots indicate 95% confidence limits; those are estimated from the variance in the information contributed to the bin from each of the 70 different microstructures. Local density follows a sigmoidal profile at the surface. No chain layering (oscillatory behavior in the total density profile) is obvious within the error of the simulation. In this respect, our glassy polymer surface is reminiscent of the free surfaces of simple liquids, at which the absence of layering has been confirmed.[20] A very recent Monte Carlo simulation of the free surface of a melt consisting of freely jointed bead–spring chains[2] also shows no evidence of layering. One way of characterizing interfacial thickness is through the distance over which mass density falls from its bulk value to practically zero. With this definition, we find the thickness of a glassy polymer/vacuum interface to be less than 10 Å. While this thickness may increase somewhat in the presence of

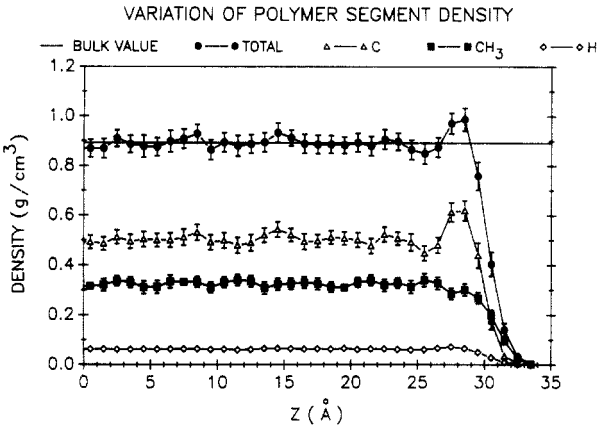

Figure 5. Local mass density distribution at a glassy polymer–vacuum interface. Vacuum is located at the extreme right, and the region near $z = 0$ is representative of unperturbed bulk polymer. The solid line indicates the experimentally observed macroscopic density at the simulation temperature. Individual contributions to the mass density profile from carbon, hydrogen, and methyl atoms are also shown.

thermal motion, it is significantly smaller than overall chain dimensions. The bulk density under the simulation conditions is indicated in Figure 5 as a thin line. Evidently, the middle region of the model film (around $z = 0$) is indistinguishable from bulk polymer in terms of density. Also shown in Figure 5 are the individual components of mass density, due to the three atomic species present in the system. Interestingly, there is a tendency for species to segregate at the surface. The highly attenuated surface region is enriched in methyl groups. As one moves into the bulk, the density distribution of methyls rises slowly in a sigmoidal fashion. On the contrary, the density distribution of carbons rises steeply, displaying a shallow peak around $z = 28$ Å. Density profiles obtained for the short-chain ($x = 25$) system are practically indistinguishable from those of Figure 5 and are therefore not shown here. This indicates that the density distribution is insensitive to chain size and is governed by length scales characteristic of individual chain segments. A similar conclusion concerning polymer melts has been arrived at via a self-consistent field lattice model.[13]

Local bond orientational tendencies induced by the presence of surfaces constitute another interesting structural aspect. To characterize bond orientation we define an order parameter, averaged over all bonds whose midpoint lies within a given "bin", and over all model structures:

$$S_B = {}^1/_2[3\langle\cos^2\theta\rangle - 1] \quad (3)$$

In eq 3, θ is the angle measured between the z axis and the bond under examination, and $\langle\ \rangle$ is indicative of averaging over all microstates within the bin. S_B equals 0, 1, and $-{}^1/_2$ for bonds with perfectly random, perpendicular, and parallel orientations relative to the surface plane, respectively. S_B profiles were accumulated separately for skeletal C–C, pendant C–H, and pendant C–CH_3 bonds using 2-Å-thick bins. Results, shown in Figure 6, indicate that all bonds are randomly oriented in the bulk, as expected. In the vicinity of the free surface, backbone bonds exhibit a weak tendency for parallel orientation over the same region in which the sigmoidal drop in density is observed. S_B(C–C) displays a minimum a few angstroms away from the extreme edge of the film; this suggests a tendency for chains to run parallel to the surface and thereby maximize favorable cohesive interactions with chains in the interior of the film. In other

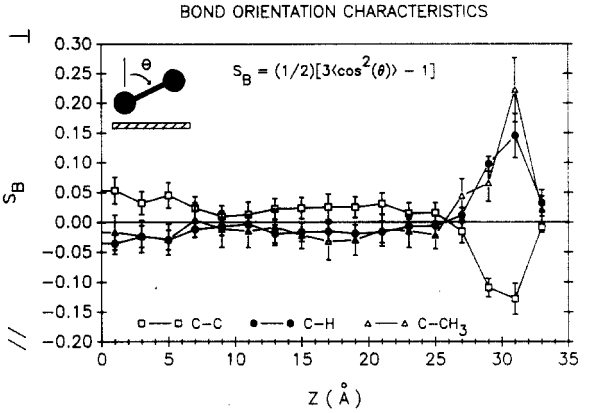

Figure 6. Local order parameter for C–C, C–H, and C–CH_3 bonds as a function of distance from the film midplane. A positive (negative) order parameter indicates an orientational tendency that is perpendicular (parallel) to the surface planes.

words, backbones are reluctant to venture into the highly attenuated surface region and would rather cling to the bulk. In the bin closest to the vacuum phase, where the polymer is highly attenuated, S_B(C–C) reverts to less negative values. Backbones do not have much to gain by adhering to underlying chains, and orientational disorder sets in. The shallow minimum in S_B is consistent with the predictions of a self-consistent-field model of polymer melt surfaces.[13] That model actually predicts that S_B will ultimately become positive at the extreme edge of a melt, due to a tendency of chain tails to stick out into the vacuum phase; such a perpendicular orientation is not seen in our static glassy microstates. The order parameter of pendant bonds is opposite in sign and roughly equal in magnitude to that of skeletal bonds in the interfacial region. Again, it is remarkable that bond orientation effects are quite short-ranged. Randomness prevails roughly 10 Å into the film from the extreme edge of the polymer. By comparing against the shorter chain system (results not shown here), we established that bond orientation effects are insensitive to molecular weight.

Polymer chains in the amorphous bulk resemble unperturbed chains. The distribution of their skeletal bond torsion angles among various conformational states has been found[8] to be close to the corresponding distribution for isolated chains under Θ conditions (Flory's random coil hypothesis). The constraints imposed on chain organization in the interfacial region may cause the conformational preferences of chains to depart from what they are in the bulk. To assess this effect, we undertook a study of the distribution of bond torsion angles as a function of position of the bond midpoints. Within each 1-Å-thick bin, rotation angles were grouped into five rotational states, defined according to the rotational isomeric state scheme of Suter and Flory.[15] The intervals used in assigning angles to rotational states are the same as in ref 8. The frequency of each state was calculated in each bin. The distribution of torsion angles accumulated in the middle region of our model film is entirely consistent with previous bulk work[8] (Figure 7); the t state is most favored, followed by g. The profiles of Figure 7 indicate that significant conformational perturbations occur in the surface region. The relative frequency of the t state decreases, and a corresponding enhancement in the g and $\bar{g}$ states is observed. These states, ordinarily not favored due to high short-range intramolecular energy, nevertheless allow a chain to quickly turn back from the vacuum into the energetically more favorable bulk. Perturbations from bulk behavior are again observed over a narrow region, less than 10 Å thick, and are not chain length dependent.

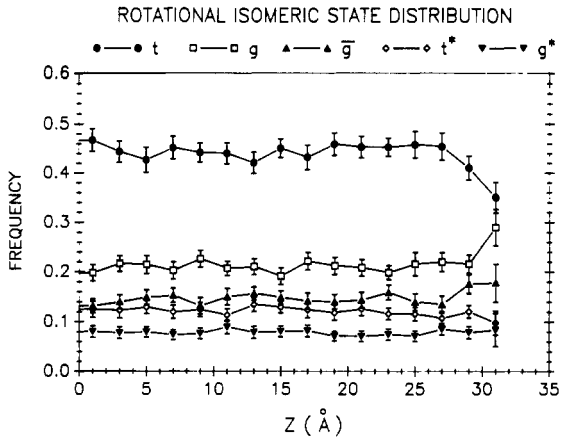

Figure 7. Distribution of torsion angles, assigned to their nearest rotational isomeric state value, as a function of position in the film. A depletion in the usually most favored t state is observed at the interface.

In addition to local structure at the level of segments and bonds, longer range structural features at the level of entire chains are of interest. An important length scale at this level of description is provided by the chain's radius of gyration. In the glassy bulk, our 152-bond atactic polypropylene chains have a root mean squared radius of gyration $\langle s^2 \rangle^{1/2} = 17.2 \pm 2.1$ Å (all errors correspond to 95% confidence limits); this is close to the rotational isomeric state model value $\langle s^2 \rangle_0^{1/2} = 18.8 \pm 0.1$ Å for unperturbed chains.[8] The radius of gyration of the 50-bond-long atactic polypropylene chains, estimated from the central region of our low molecular weight model film, is $\langle s^2 \rangle^{1/2} = 9.03 \pm 0.25$ Å; this is not far from the value $\langle s^2 \rangle_0^{1/2} = 9.85 \pm 0.04$ Å calculated with the rotational isomeric state model. The extent to which we can explore structure at the level of entire chains is, of course, limited by the small size of our systems. For example, periodic boundary conditions in the x and y directions enforce artificial peaks in the pair distribution function of chain centers of mass at approximately 17 Å. Given the diffuse nature of chain segment clouds, which can interpenetrate profusely, we would not expect this artificial periodicity to have serious consequences on chain shape, size, and orientation. Bulk simulations, carried out in the past under the same limitations,[8] resulted in very good agreement with reality. Furthermore, comparisons between our long-chain and short-chain systems immediately point out any existing system size effects (see below).

An interesting question is how chains, as entire objects, distribute themselves in the interfacial region. To address this question we accumulated the singlet density distribution function of chain centers of mass, using 4-Å-thick bins. Results for the $x = 76$ and $x = 25$ systems are displayed in parts a and b of Figure 8, respectively. The uniform distribution that would prevail in the isotropic bulk is also drawn in the same figure, for comparison. In contrast to the segment density distribution of Figure 5, the distribution of centers of mass shows considerable structure. There is a depletion of centers of mass in the surface region, followed by a pronounced peak at roughly one radius of gyration away from the extreme edge of the film. The physical reason for this is simple: Chains are objects of finite dimensions; therefore their center of mass cannot be arbitrarily close to the surface. Clearly, structure at the level of entire chains is governed by length scales characteristic of overall chain size, rather than segment size; the location of the peak is significantly different between Figure 8a and Figure 8b. In the larger chain system structure appears somewhat sharper. In all

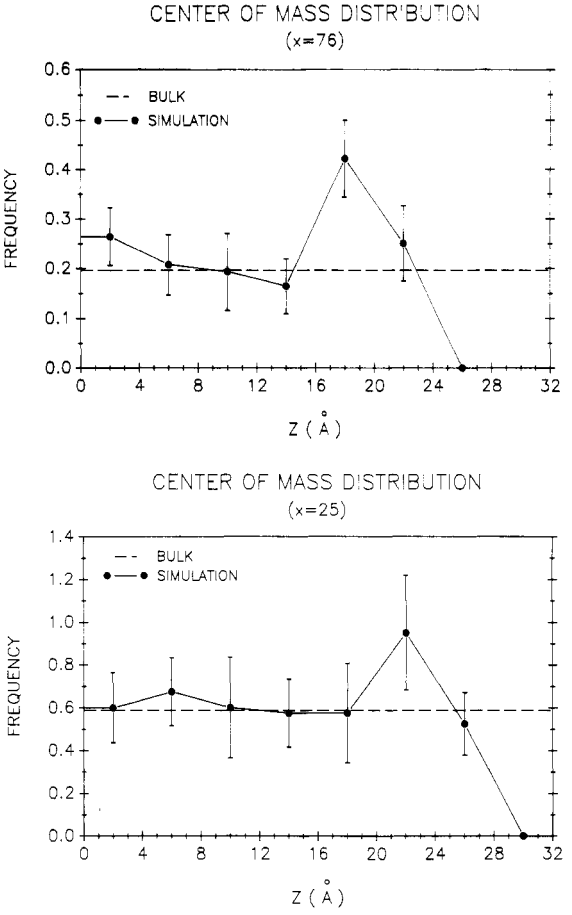

Figure 8. Chain center of mass distribution, accumulated in 4-Å-thick bins: ((a) top) $x = 76$ system; ((b) bottom) $x = 25$ system. A peak appears roughly one radius of gyration from the edge of the film.

likelihood, this is a consequence of the small size of the model box in the x and y directions relative to the chain (see below); periodic images of the surface chains are less than a radius of gyration apart and would thus occupy most of the surface region, limiting the extent to which other chains can approach the surface. The more diffuse profile of Figure 8b should thus be more representative of reality. Previous Monte Carlo simulations of free polymer surfaces that involved cruder molecular lattice[1] and off-lattice[2] representations and even simulations of polymer/solid interfaces[3-7] have led to center of mass distributions that display the qualitative features of Figure 8.

A simple measure of the average shape of chains as a function of position in our model glassy films is presented in Figure 9a,b. To prepare this figure, the superposed microstructures were divided into 1-Å-thick bins. The total number of skeletal segments (i.e., terminal R, CHR, or CH_2 groups) contained in each bin was counted; so was the total number of chains passing through each bin. These two numbers were divided by each other, to arrive at the average number of segments per chain participating in each bin. This number, plotted as the ordinate in Figure 9, is indicative of the average "width" of chains at various depths of the interfacial region. As one moves into the film from the vacuum, the chain width rises to a maximum, along a sigmoidal profile spanning a distance of roughly 6 Å for both chain lengths; this is a direct consequence of the shape of the segment density profile displayed in Figure 1. Subsequently, the chain width decays to an asymptotic value characteristic of the bulk, over a distance slightly larger than one radius of gyration. The $x = 76$ profile is somewhat irregular, due to system and sample size

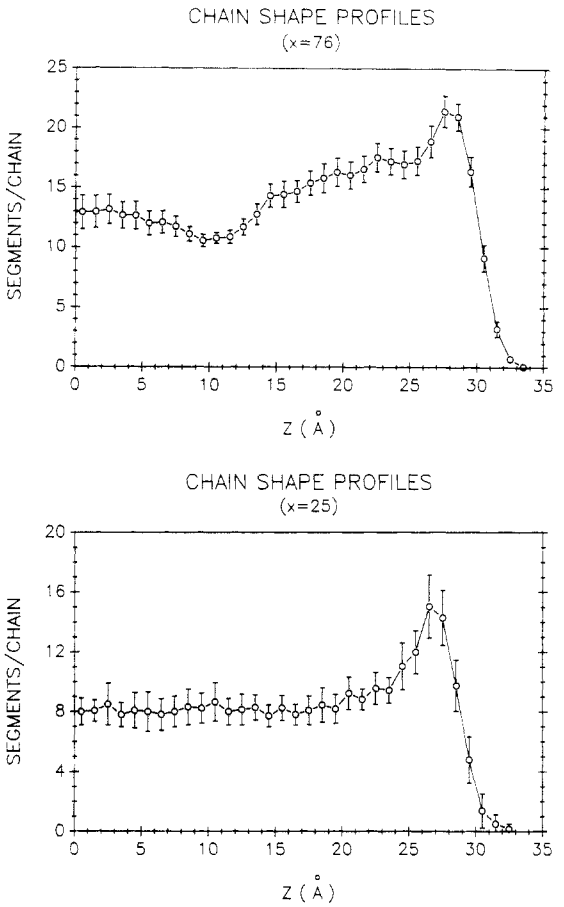

Figure 9. Average width of chains plotted as a function of position: ((a) top) x = 76 system; ((b) bottom) x = 25 system. The distribution was accumulated using 1-Å-thick bins. See text for details.

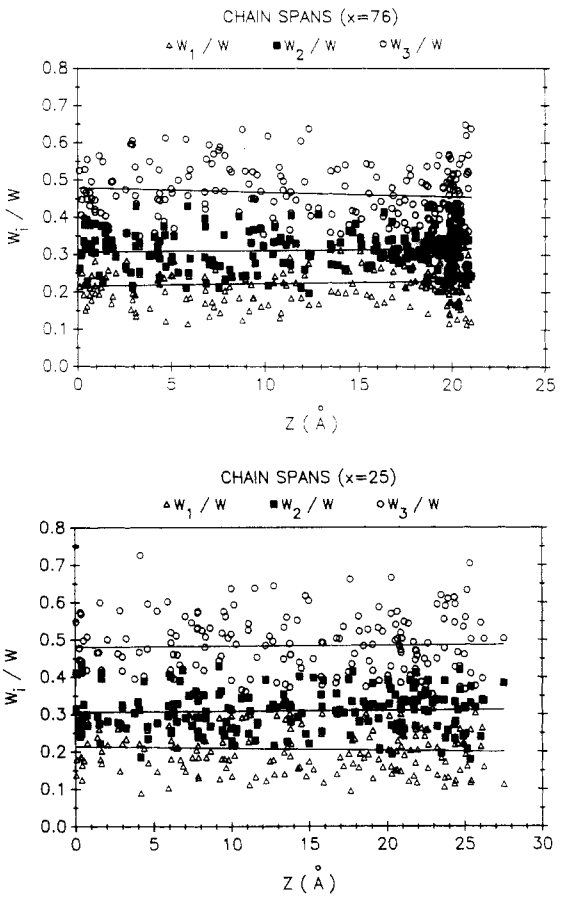

Figure 10. Spans of chains plotted against their center of mass position in the film: ((a) top) x = 76 system; ((b) bottom) x = 25 system. The sum of all three spans has been used as a normalizing factor (i.e., $W = W_1 + W_2 + W_3$). The straight lines have been drawn by least-squares regression of the data. This plot provides information on the overall shape of chain segment clouds, independent of their orientation.

limitations; in the x = 25 case, the attainment of asymptotic bulk behavior is obvious. The basic conclusion is that chains are flattened in the interfacial region. In the long-chain system, chains just below the highly attenuated region of the interface are by roughly 60% "wider" than chains in the bulk; the profile of Figure 9a is strikingly similar to what is predicted via a mean field lattice model of polymer melt surfaces (Figure 9b of ref 13). The flattening effect appears more pronounced in the shorter chain system (Figure 9b).

Is the "flattening" depicted in Figure 9 due to perturbation in the intrinsic shape of chains, or is it caused by a tendency for chains as whole objects to assume preferred orientations with respect to the surface? To answer this question, we first looked at two measures of the intrinsic shape of the chain segment cloud, namely spans and eigenvalues of the radius of gyration tensor. Following Rubin and Mazur,[21] we define the longest span W_3 as the straight line segment connecting those two skeletal atoms of the chain that are farthest apart from each other. The intermediate span W_2 is the longest straight line segment drawn in a plane perpendicular to the direction of the longest span and connecting two skeletal atoms. The shortest span W_1 is the third edge of an orthogonal parallelepiped completely enclosing the chain skeleton and drawn with the longest and intermediate spans as two of its edges. Note that by classifying chains according to the length of their spans, one does not distinguish between chains of the same shape but of different overall orientation with respect to the film frame of reference. Individual spans, normalized by the sum of all three spans, are plotted as a function of the z coordinate of the chain center of mass in Figure 10a,b. There is considerable scatter in the data, due to limited sample size. Nevertheless, one can conclude that the overall shape of chains does not change significantly as one passes from the bulk into the interfacial region. Moreover, the normalized spans are indistinguishable between the x = 76 and x = 25 systems. As an additional measure of structure, the eigenvalues $L_1^2 < L_2^2 < L_3^2$ of the radius of gyration tensor were computed by identifying the principal axis system of each chain. Normalized eigenvalues are plotted in Figure 11a,b against chain center of mass position. Again, L_1^2, L_2^2, and L_3^2 are constant throughout the interfacial region within the error of the simulations and indistinguishable from their asymptotic unperturbed random walk values[22] for both chain lengths. We are thus led to the conclusion that the intrinsic shape of the chain segment cloud remains practically unperturbed in the presence of a polymer/vacuum interface.

The measures of shape depicted in Figures 10 and 11 convey no information about the overall orientation of chains, as three-dimensional objects, in the intrinsically anisotropic environment of the surface. To explore this aspect of structure, we calculated order parameters S_w for the longest and shortest spans of our chains. Results from this calculation, using eq 3 where θ is now the angle between the z axis and the span of interest, are depicted in Figure 12a for the x = 76 system. The binning scheme in this figure is such that each bin contains 35 chain centers. In the middle region of the film, both spans appear randomly oriented (S_w = 0). In the surface region, the longest

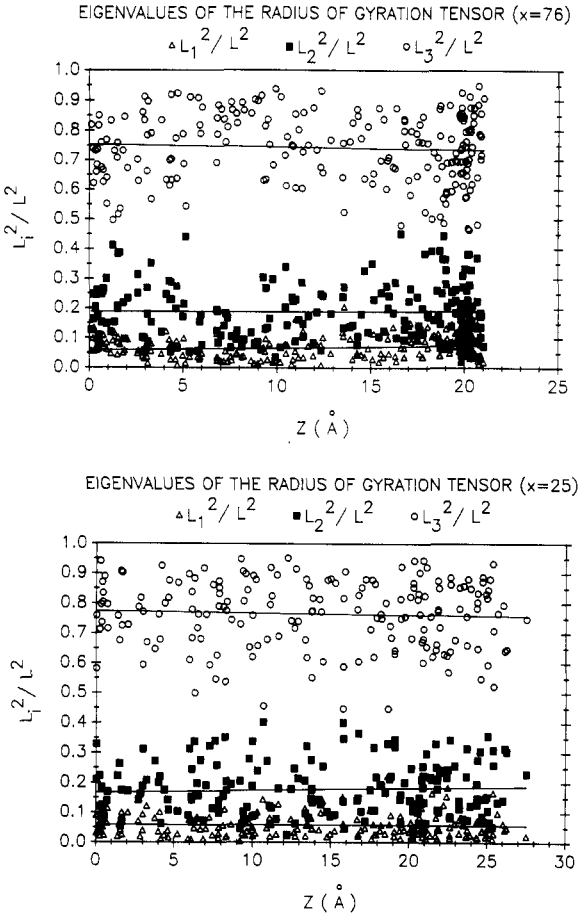

Figure 11. Eigenvalues of the radius of gyration tensor of chains plotted against their center of mass position in the film: ((a) top) $x = 76$ system; ((b) bottom) $x = 25$ system. The sum of all eigenvalues has been used as a normalizing factor (i.e., $L^2 = L_1^2 + L_2^2 + L_3^2$). Lines indicate least-squares regression results.

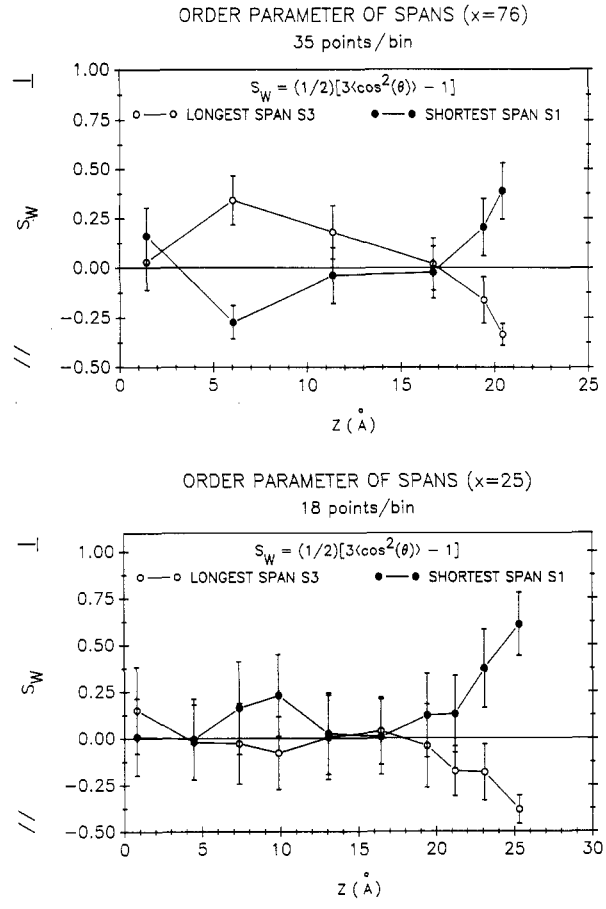

Figure 12. Order parameters for the longest and shortest spans of chains plotted against their center of mass position: ((a) top) $x = 76$ system; ((b) bottom) $x = 25$ system.

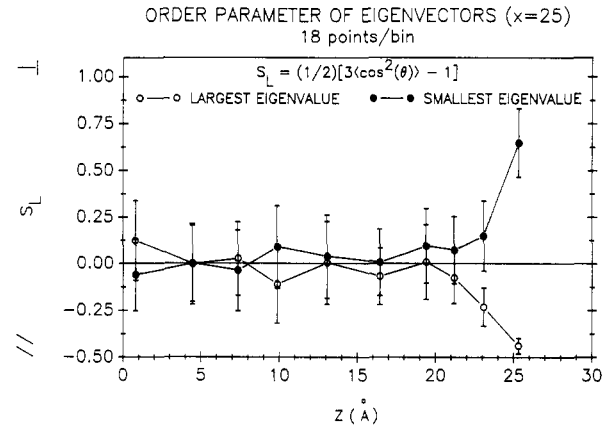

Figure 13. Order parameters for the longest and shortest principal axes (i.e., the eigenvectors corresponding to the smallest and largest eigenvalue of the radius of gyration tensor) in the $x = 25$ system.

(shortest) spans exhibit a clear tendency for parallel (perpendicular) orientation with respect to the surface. In other words, chains tend to lie flat at the surface, with their shortest dimension parallel to the z axis. Results from the shorter chain system (Figure 12b), where each bin now contains 18 chain centers, demonstrate a similar trend for surface chains to orient with their longest dimension parallel to the xy plane and for chains in the central region of the film to assume random orientations.

In between the central and surface regions, chains in the larger molecular weight system (Figure 12a) display some tendency to orient with their longest spans perpendicular to the surface. Such a tendency is absent from the shorter chain system. This is seen in Figure 12b, and even clearer in Figure 13, where order parameters for the longest and shortest principal axes of $x = 25$ chains are depicted. The orientational tendencies observed between $z = 2$ Å and $z = 15$ Å in the longer chain system are a structural artifact, linked to the small size of the simulation box relative to chain dimensions. The registry enforced by periodic boundary conditions in the x and y directions leads to the presence of chains elongated along the z direction halfway between the surface and the middle of the film. How this happens is explained schematically in Figure 14a. Direct evidence on the shape of the segment cloud in different regions of the longer chain system is presented in Figure 14b. To prepare this figure, all chains encountered in our $x = 76$ model microstructures were divided into three groups, according to their center of mass position. Within each group, chains were translated parallel to the x, y, and z axes so that their centers of mass coincided. Three-dimensional contour plots of the segment density distribution, which is cylindrically symmetric around the z axis, were then created.[23] As expected from our discussion of Figures 9a and 12a above, chains are flattened in the surface region. Near the film midplane, the orientational distribution of chains becomes uniform, so their rotationally averaged shape is spherical. Halfway between the surface and the midplane, some tendency for chains to assume a prolate ellipsoidal shape, elongated along the z axis, is indeed observed. Our shorter chain simulations are free of this artifact. In both the short- and the long-chain cases, the tendency for segment clouds to lie flat on the surface is the primary noteworthy structural feature.

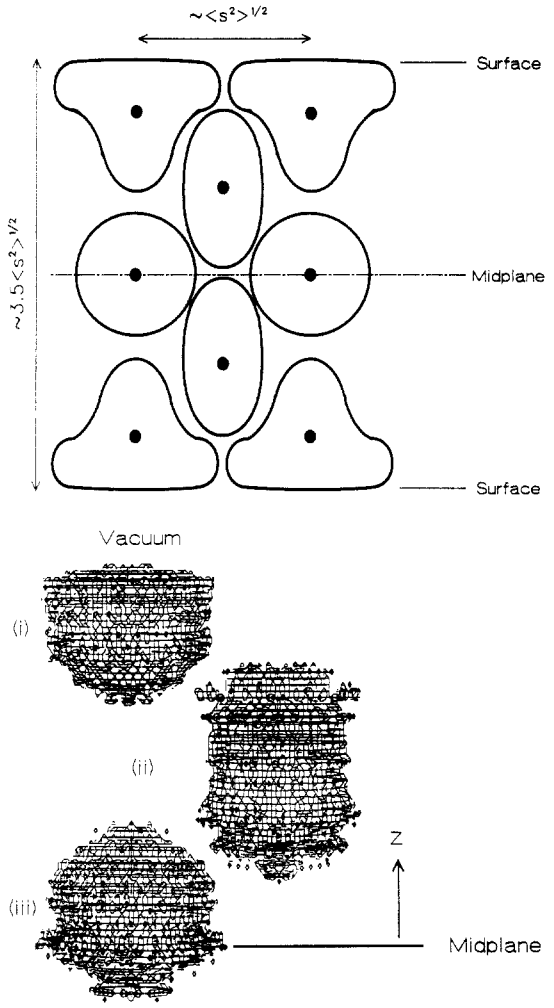

Figure 14. ((a) Top) Schematic representation of the orientation of chains in the long chain (x = 76) system. $\langle s^2\rangle^{1/2}$ stands for the radius of gyration of chains in the bulk. The approximate dimensions of the periodic box are indicated. The contours convey the approximate shape of the segment cloud of chains participating in each region of the film as it would appear after rotational averaging around the z axis. The ordering imposed by periodic boundary conditions leads to the appearance of chains elongated perpendicular to the surface, midway between the surface and the film midplane. ((b) Bottom) Average shape of the segment cloud of chains participating in various regions of the longer chain (x = 76) film. Average shapes are symmetric with respect to rotation around the z axis. Contours are drawn at a constant value of segment density, equal to 0.003 segments/Å^3. To study shape, chains were divided into the following three categories according to the distance z_{COM} of their centers of mass from the film midplane: (i) z_{COM} larger than 16 Å ("surface chains"); (ii) z_{COM} between 4 and 16 Å; (iii) z_{COM} less than 4 Å ("bulk chains"). Contour plots were drawn using ref 23.

Thermodynamics. The atomistically detailed representation we employ in this work was designed so as to allow the prediction of experimentally measurable surface thermodynamic properties. An important thermodynamic quantity that can be derived from our set of static model microstates is the internal energy contribution to surface tension.

A macroscopic thermodynamic analysis of the glassy polymer/vacuum interface can be formulated as follows: Consider a one-component system consisting of a flat film of glassy polymer in equilibrium with its vapor. The vapor phase is isotropic at a pressure P, which, of course, will be extremely low due to the involatility of the polymer. The whole system is at a temperature T, and the chemical potential of the polymer is μ. We will assume that the film is sufficiently thick so that its central region is indistinguishable from bulk polymer. In view of the structural results reported in the previous section, this would be a reasonable approximation even for films as thin as 61 Å. We partition the entire system into an isotropic vapor phase and a film phase. The latter contains the entire anisotropic region of surface polymer as well as the isotropic region in the middle. The fundamental equation for the film phase in the energy representation is[13,24]

$$\mathrm{d}\underline{U} = T\,\mathrm{d}\underline{S} - P\,\mathrm{d}\underline{V} + \mu\,\mathrm{d}n + \gamma\,\mathrm{d}\underline{a} \tag{4}$$

where $\underline{S}$, $\underline{V}$, n, and $\underline{a}$ stand for entropy, volume, number of moles, and total surface area (both sides), respectively. γ is the surface tension. The notational convention of Modell and Reid[25] is followed here, whereby all extensive properties other than mole numbers are underlined. Introducing the Helmholtz energy $\underline{A}$ as the first Legendre transform of internal energy with respect to entropy, we obtain

$$\mathrm{d}\underline{A} = -\underline{S}\,\mathrm{d}T - P\,\mathrm{d}\underline{V} + \mu\,\mathrm{d}n + \gamma\,\mathrm{d}\underline{a} \tag{5}$$

hence

$$\gamma = \left.\frac{\partial \underline{A}}{\partial \underline{a}}\right|_{T,\underline{V},n} = \left.\frac{\partial \underline{U}}{\partial \underline{a}}\right|_{T,\underline{V},n} - T\left.\frac{\partial \underline{S}}{\partial \underline{a}}\right|_{T,\underline{V},n} = \gamma^U + \gamma^S \tag{6}$$

In eq 6, γ is separated into an internal energy γ^U and an entropic contribution γ^S. Furthermore, by a Maxwell relation on eq 5, it can be shown that $\gamma^S = T\,\partial\gamma/\partial T|_{V,n,\underline{a}}$. A rearrangement of eq 6, combined with this result, gives

$$\gamma^U = \left.\frac{\partial \underline{U}}{\partial \underline{a}}\right|_{T,\underline{V},n} = \gamma + T\left.\frac{\partial \underline{S}}{\partial \underline{a}}\right|_{T,\underline{V},n} \approx \gamma - T\frac{\mathrm{d}\gamma}{\mathrm{d}T} \tag{7}$$

An alternative thermodynamic analysis, which clarifies the meaning of eq 7, is presented in Appendix D. The right-hand side of eq 7 is experimentally measurable. On the other hand, the derivative $\partial\underline{U}/\partial\underline{a}|_{T,\underline{V},n}$ can be estimated for each of our model glassy microstates as the corresponding derivative $\partial\mathcal{V}^0/\partial\underline{a}|_{\underline{V},n}$ of potential energy (Appendix A). All one needs to do in order to obtain $\partial\mathcal{V}^0/\partial\underline{a}|_{\underline{V},n}$ is subject the microstate to a very small volume-preserving deformation that dilates the surface area $\underline{a}$ while keeping total volume constant, relax to a new energy minimum, monitor the associated change in potential energy $\mathcal{V}_0$, and estimate the derivative $\Delta\mathcal{V}^0/\Delta\underline{a}|_{\underline{V},n}$ by finite differences. Furthermore, it has been established in our previous bulk work[9] and confirmed in these interfacial investigations (Appendix D) that the change in potential energy brought about by a small deformation of a minimum-energy structure remains practically the same if the deformation is imposed in an *affine* manner, i.e., if all atom coordinates are transformed by a linear rule. An analysis of the energetic consequences of an infinitesimal *affine* deformation that changes $\underline{a}$ but preserves the value of $\underline{V}$ led to the following analytical expression for γ^U:

$$\gamma^U = -\frac{1}{2\underline{a}}\Big\langle \sum_i \sum_{\substack{j\neq i \\ i,j \text{ in box}}} \big[{}^1/_2 F^{\min}{}_{ij,x}(x_i - x_j)_{\min} + {}^1/_2 F^{\min}{}_{ij,y}(y_i - y_j)_{\min} - F^{\min}{}_{ij,z}(z_i - z_j)\big]\Big\rangle \tag{8}$$

A derivation of this expression is presented in Appendix E. In eq 8, x_i, y_i, and z_i stand for atomic coordinates. $\mathbf{F}_{ij}$ is the total force between i and j, including bonded contributions.[9] The symbol min denotes minimum image atom pairs. The angular brackets indicate that an estimate of γ^U for the real glass is obtained by arithmetically

averaging estimates from individual microstructures. Equation 8 is closely related to eq 65 of ref 9 for calculating the components of internal stress. It was pointed out that the internal stress equation is a static analogue of the virial theorem for the stress tensor. In the same way, eq 8 is a static analogue of the virial theorem for surface tension[26] that has been used to estimate γ through molecular dynamics simulations of simple liquids and low molecular weight fluids.[24,27] In order to use eq 8, bonded forces were calculated by solving the detailed force and torque balance equations along each chain, as described in ref 9. It is possible to derive an expression for γ^U equivalent to eq 8, but cast exclusively in terms of *nonbonded* interatomic forces (see Appendix F). This expression, unlike eq 8, does not require knowledge of the bonded forces and is therefore more general.

To arrive at a realistic estimate for γ^U, it is necessary to incorporate "potential tail" contributions. By "potential tails" we mean interactions over distances larger than the interatomic potential ranges[9] used in the molecular mechanics calculation. The tail contribution in each structure was arrived at by direct integration, based on "smearing" the atomic density distribution in the x and y directions; a detailed derivation is presented in Appendix G.

Our final prediction for γ^U, based on the set of 70 microstructures of degree of polymerization $x = 76$, is (average ± 95% confidence limits)

$$\gamma^U_{\text{theory}} = 43 \pm 23 \text{ mN/m} \quad (9)$$

The large magnitude of the error reflects limited sample size. Experimental values for the surface tension of atactic polypropylene at 20 °C (γ = 29.4 mN/m), 140 °C (γ = 22.7 mN/m), and 180 °C (γ = 20.4 mN/m) are given by Wu (ref 28, p 88). It has been found empirically (ref 28, p 67) that the relation between γ and T in a melt is linear within not too wide temperature ranges and can be extrapolated to temperatures below the glass transition temperature. Such an extrapolation, based on the above surface tension values, yields the experimental estimate

$$\gamma^U_{\text{exp}} = 45.9 \pm 02 \text{ mN/m} \quad (10)$$

In view of eqs 9 and 10, we conclude that our atomistic simulation can predict γ^U, a measurable thermodynamic property, within 7% of experiment.

5. Summary and Conclusions

Detailed atomistic computer simulations were performed on a thin glassy polymer film to (a) elucidate microscopic aspects of structure and molecular organization at a "free" polymer surface and (b) predict an interfacial thermodynamic property (the internal energy contribution to surface tension) directly from the geometry and energetics of chains making up the film. The simulation is based on the hypothesis that the glassy film can be represented as a set of static microstructures "locked" in a state of detailed mechanical equilibrium, i.e., at a local minimum of the total potential energy with respect to all microscopic degrees of freedom. An efficient computational procedure based on Monte Carlo and energy minimization techniques has been designed to generate such a set and applied to the case of a 61.17-Å-thick film of glassy atactic polypropylene at −40 °C.

Local structural features at the free polymer surface were analyzed at the level of individual segments and bonds and at the level of whole chains. The segment density falls from its bulk value to zero along a sigmoidal profile. Skeletal bonds tend to align parallel to the surface. The distribution of bond torsion angles is perturbed relative to the bulk, exhibiting a depletion in the usually favorable t conformational state near the surface. These traits extend over a distance of less than 10 Å from the extreme edge of the film; they are insensitive to the molecular weight of the polymer. The average width of chains in directions parallel to the film midplane is significantly larger near the surface than in the bulk. The intrinsic shapes of chain segment clouds, as characterized by spans and the eigenvalues of the radius of gyration tensor, do not depart much from those encountered in the bulk polymer. Chains do tend to organize, however, with their longest span parallel and their shortest span perpendicular to the surface plane. The center of mass distribution displays a peak roughly one radius of gyration from the extreme edge of the polymer. Structural features at the level of entire chains are governed by a length scale commensurate with the radius of gyration.

The internal energy contribution to surface tension, $\gamma^U = \partial \underline{U}/\partial \underline{a}|_{T,V,n}$, was predicted from the energy changes accompanying an infinitesimal affine deformation that dilates the area of each microstructure, while preserving its total volume. Our result, which is the first estimate of an interfacial thermodynamic property to be reached by first-principles molecular simulation of a polymer system, is within 7% of the corresponding experimental value.

To keep computations tractable, thermal motion has been factored out of this simulation work. Our model films are pictured as completely glassy throughout their entire thickness. In reality, the lower density prevailing at the extremities of the film should give rise to some segmental mobility, which should be damped as one moves into the denser bulk. Even though our picture of a completely glassy free surface is not absolutely accurate, it should capture the essential features of surface structure and thermodynamics quite satisfactorily. This is evidenced by the favorable agreement of the predicted value of the internal energy contribution to surface tension with experiment. Future work will involve the introduction of thermal fluctuations into our simulation methodology through the implementation of molecular dynamics techniques. By incorporating thermal motion into our atomistic model, we will be able to predict the surface tension γ (and not only its internal energy contribution) from first principles.

Acknowledgment. We acknowledge the generous support provided for this work by the Director, Office of Energy Research, Office of Basic Energy Sciences, Materials Science Division of the U.S. Department of Energy under Contract DE-AC03-76SF00098; by the British Petroleum Corp.; and by the Union Carbide Corp. We are grateful to Cray Research, Inc., for generous financial and computational support. We thank the San Diego Supercomputer Center, where all computations were performed, for excellent technical support. D.N.T. expresses gratitude to the National Science Foundation for a 1988 Presidential Young Investigator Award, No. DMR-8857659.

Appendix A. Statistical Mechanics of a Glassy Polymer Film

Consider a glassy film of thickness sufficiently large so that isotropic conditions prevail in its middle region. Our atomistic modeling approach is essentially an extension to anisotropic systems of a microscopic picture invoked in the past for the prediction of bulk structure and elastic properties.[8,9] It rests on the following assumptions:

A1. The polymer is involatile; the density of chains that would be present in a gas phase at equilibrium with the film is extremely low, and does not affect the thermodynamics of the film.

A2. The film is glassy throughout its entire extent. A glass (see Introduction) is envisioned here as locally consisting of solidlike microstates, each "locked" in the vicinity of a local minimum of total potential energy in configuration space. The microstates are mutually inaccessible; transitions between neighboring minima in configuration space are inhibited by high energy barriers. Estimates of thermodynamic properties are obtained by arithmetically averaging the properties of individual microstates. The distribution of minimum-energy microstates encountered in an actual glass would, of course, depend on the history of vitrification. We assume here that our method of generating liquidlike initial-guess configurations and subsequently relaxing them by energy minimization yields a sufficiently accurate representation of a real glass formed by slowly cooling a melt.

A3. The bond lengths and bond angles (hard degrees of freedom) of our model chains are treated as classical springs of very high stiffness. In ref 8 we have presented an analysis of vibrational motion associated with the hard degrees of freedom. It was concluded that the quantum nature of thermal motion does not significantly affect the values of thermodynamic properties related to the spatial extent of the system, such as stress, elastic constants, and surface tension, at the temperatures of interest here.

Our minimum-energy microstates are reminiscent of the potential energy minima considered by Stillinger and Weber[29] in their studies of inherent structure in small-molecule amorphous materials. According to these authors, the bulk structure of liquids and glasses arises mostly from thermal stimulation of an underlying family of 0 K quenched structures. A difference between our microstates and those of Stillinger and Weber is that our minimum-energy microstates are created at a specific bulk density and therefore refer to a specific set of temperature and pressure conditions. Although stripped of thermal motion, our microstates are not 0 K structures; by construction, their bulk region has a density characteristic of −40 °C. The average diagonal elements of the internal stress tensor (see Appendix E) are strongly positive (tensile) in our model system, reflecting cohesive interactions in the polymer. One could readily introduce thermal motion in each of our microstates by initiating a Monte Carlo or molecular dynamics simulation. This would entail injecting energy into the model system so as to cause it to explore the potential energy well at whose bottom a static microstate resides. Momentum contributions to stress would more than offset the tensile internal stress; the resulting normal pressure and transverse pressure distributions would reflect the pressure state experienced by an actual glassy polymer film characterized by the temperature and density distribution used in our static simulation. Sylvester, Yip, and Argon[30] have recently performed isothermal–isostress molecular dynamics simulations below and above the glass transition temperature, starting from bulk polypropylene microstates generated by our static simulation method.[8] Their predictions for volumetric behavior, solubility parameter, heat capacity, and X-ray structure factors are in excellent agreement with experiment and consistent with our previous static simulation results.

Under assumption A1, we can deal with the statistical mechanics of our film independently from the gas phase, within the framework of the canonical ensemble. Under assumption A3 ("classical flexible model"; see refs 32 and 33), the partition function of our film, consisting of N_c chains, each containing $(6x - 1)$ atoms, can be written as

$$Z = \frac{1}{N_c!}\left\{\left[\prod_{\alpha=1}^{6x-1}\left(\frac{m_\alpha}{2\pi\beta\hbar^2}\right)^{3/2}\right]\left(\frac{2\pi}{\beta}\right)^{(16x-7)/2} \times \left[\frac{1}{\det \mathbf{F}''}\right]^{1/2}\right\}^{N_c}\prod_{k=1}^{N_c} D_0^{(k)} \int \exp\{-\beta\mathcal{V}(\mathbf{q}_1,\mathbf{q}_2,...,\mathbf{q}_{N_c})\}\prod_{k=1}^{N_c} d\mathbf{q}_k \quad (A.1)$$

In eq A.1, $\mathbf{F}''$ is a $(16x - 7) \times (16x - 7)$ matrix of force constants associated with the hard degrees of freedom. $D_0^{(k)}$ is the Jacobian of the transformation from atomic Cartesian coordinates of chain k to generalized coordinates; it is evaluated keeping all hard degrees of freedom of chain k at their equilibrium values and depends only on bond lengths and bond angles. $\mathcal{V}$ is the total potential energy of the system, expressed as a function of the "soft" degrees of freedom of the chains, all hard degrees of freedom being kept at their equilibrium values. $\mathbf{q}^{(k)} = (\mathbf{r}_0^{(k)},\psi^{(k)},\phi^{(k)})$ symbolizes collectively the soft degrees of freedom of chain k. The expression we use for $\mathcal{V}$ is given by eq C.1.

By assumption A3, chains within a small region of the glassy film are not free to explore the entire configuration space available to them over reasonable time scales. Rather, they are restricted to configurations around a local minimum $\mathcal{V}^0(\mathbf{q}_1^0,...,\mathbf{q}_{N_c}^0)$. Moreover, the small deformations of interest in the definition of the surface tension cannot cause the system to depart from the set of minima in which it resides. We can therefore formulate a local thermodynamics around each minimum-energy microstate as we would do for a crystalline solid.[8,31] Over the region of configuration space around a minimum-energy state, we can approximate the potential energy function by[9]

$$\mathcal{V}(\mathbf{q}_1,\mathbf{q}_2,...,\mathbf{q}_{N_c}) = \mathcal{V}^0 + (\mathbf{g}^0)^T\begin{bmatrix}\mathbf{q}_1 - \mathbf{q}^0{}_1\\ \vdots \\ \mathbf{q}_{N_c} - \mathbf{q}^0{}_{N_c}\end{bmatrix} + \frac{1}{2}[(\mathbf{q}_1 - \mathbf{q}^0{}_1)^T,...,(\mathbf{q}_{N_c} - \mathbf{q}^0{}_{N_c})^T]\mathbf{H}^0\begin{bmatrix}\mathbf{q}_1 - \mathbf{q}^0{}_1\\ \vdots \\ \mathbf{q}_{N_c} - \mathbf{q}^0{}_{N_c}\end{bmatrix} \quad (A.2)$$

In eq A.2, $\mathbf{g}^0$ is the $N_c(2x + 4)$-long gradient vector, and $\mathbf{H}^0$ is the $N_c(2x + 4) \times N_c(2x + 4)$ Hessian matrix of second derivatives, both evaluated at the minimum. The gradient term of eq A.2 is zero by virtue of the fact that $(\mathbf{q}_1^0,...,\mathbf{q}_{N_c}^0)$ is a local minimum of $\mathcal{V}$.

Substituting A.2 into A.1, the partition function reduces to

$$Z = \frac{1}{N_c!}\left\{\left[\prod_{\alpha=1}^{6x-1}\left(\frac{m_\alpha}{2\pi\beta\hbar^2}\right)^{3/2}\right]\left(\frac{2\pi}{\beta}\right)^{(18x-3)/2} \times \left[\frac{1}{\det \mathbf{F}''}\right]^{1/2}\right\}^{N_c}\prod_{k=1}^{N_c} D_0^{(k)}\left[\frac{1}{\det \mathbf{H}^0}\right]^{1/2} \exp(-\beta\mathcal{V}^0) \quad (A.3)$$

The internal energy of the film is given by

$$\underline{U} = -\partial \ln Z/\partial\beta \quad (A.4)$$

Equations A.3 and A.4 lead immediately to

$$\underline{U} = \mathcal{V}_0 + N_c(6x - 1)\frac{1}{2\beta} \tag{A.5}$$

The second term in eq A.5 is a simple equipartition result arising from the classical treatment of all degrees of freedom. It is, of course, not accurate but does not affect estimates of properties such as the internal stress tensor[9] and the internal energy contribution to surface tension.

Let ξ stand for any space-related thermodynamic property, such as surface area or volume. From eq A.5, we obtain

$$\left.\frac{\partial \underline{U}}{\partial \xi}\right|_{T,\xi',n} = \left.\frac{\partial \mathcal{V}^0}{\partial \xi}\right|_{\xi',n} \tag{A.6}$$

In other words, isothermal spatial derivatives of the internal energy can be estimated by the corresponding derivatives of the potential energy, at the minimum, in the vicinity of which a glassy microstate is locked. Our estimate of γ^U is based on eq A.6, with $\xi = \underline{a}$ and $\xi' = \underline{V}$.

Appendix B. Multichain Conformation Generation by a Two-Bond Equivalent Markov Process

Chains in the amorphous polymeric bulk have been shown to be similar, on the average, to chains under Θ conditions. The objective of our initial-guess generation procedure is to obtain liquidlike microstates characterized by (i) close to unperturbed conformation in their bulk (central) region and (ii) low potential energy. In previous work[8] we have developed a "modified Markov" scheme for the Monte Carlo generation of initial-guess microstates in the isotropic bulk. This scheme blends long-range interatomic interactions with the conformational statistics of unperturbed chains, as described by the rotational isomeric state theory (RIS).[16,17] Although very effective in producing bulk model chains, our initial-guess scheme has difficulty generating conformations of chains in the vicinity of the steep repulsive walls used here (see Figure 2 and eq 1). The five rotational states of polypropylene do not always provide the polymer sufficient freedom to avoid a steep obstacle, such as the wall, when its presence is not felt until the chain is within one bond length from it. To solve this problem we developed a new method, which is based on a two-bond equivalent Markov process. The basic idea behind the new method is to consider the energetic consequences of placing both bond i and bond $i + 1$ in all combinations of states accessible to them before choosing the state of bond i. Let $q_{\zeta\xi\eta;i,i+1}$ be the conditional probability of placing bonds i and $i + 1$ in states ξ and η, given that bond $i - 1$ is in state ζ. This probability is readily calculated from RIS theory by matrix multiplication operations. The conditional probability used in this work for choosing the state of bond i is then

$$q'_{\xi;i} = \frac{\sum_{\eta} q_{\zeta\xi\eta;i,i+1} \exp\left\{-\dfrac{\Delta\mathcal{V}^{LR}{}_{\xi\eta;i,i+1} + \Delta\mathcal{V}^{W}{}_{\xi\eta;i,i+1}}{RT}\right\}}{\sum_{\xi'}\sum_{\eta} q_{\zeta\xi'\eta;i,i+1} \exp\left\{-\dfrac{\Delta\mathcal{V}^{LR}{}_{\xi'\eta;i,i+1} + \Delta\mathcal{V}^{W}{}_{\xi'\eta;i,i+1}}{RT}\right\}} \tag{B.1}$$

$\Delta\mathcal{V}^{LR}{}_{\xi\eta;i,i+1}$ corresponds to the increase in long-range polymer–polymer interaction energy upon the addition of the atoms attached to bonds i and $i + 1$ (two skeletal atoms and four substituents) into the box; it includes contributions from the same chain (defined exactly as in ref 8) and from other chains. $\Delta\mathcal{V}^{W}{}_{\xi\eta;i,i+1}$ is the increase in chain–wall interaction energy upon the addition of bonds i and $i + 1$ into the box. The advantage of the new scheme is that it allows the chains to appreciate the presence of the wall when still two bonds away. The generation of all chains in our multichain system proceeds in parallel, one bond being added at a time. That is, bond i ($i \geq 2$) is placed for chains 1, 2, ..., N_c, based on the interactions of the atoms attached to bonds $(i, i + 1)$ of the considered chain with everything already placed in the box. Subsequently, bond $i + 1$ is placed for chains 1, 2, ..., N_c by considering the energetic consequences of placing bonds $(i + 1, i + 2)$ in the box. This process continues until bond $2x - 1$ of chain N_c has been added. A single-bond scheme is used, of course, for the placement of the last rotatable bond (bond $2x - 1$) of each chain.

Appendix C. Total Potential Energy Function and Its Gradient

With the same notation conventions as in previous work (ref 8, Appendix 1), the total potential energy function for our multichain system, sandwiched between two walls, is modeled by the sum

$$\mathcal{V}(\mathbf{r}_0,\phi,\psi) = \sum_{\substack{k,\text{ parent}\\ \text{chains}\\ k>1}} \{ \sum_{\substack{i;k,\text{ bonds}\\ \text{of parent}\\ \text{chain } k\\ 2\leq i;k\leq 2x-1}} \mathcal{V}_\varphi(\phi_{i;k}) + \sum_{\substack{1;k,\text{ atoms}\\ \text{in unit cell}\\ \text{belonging to an}\\ \text{image of chain } k}} \mathcal{V}^{W}(\mathbf{r}_{1;k}) + \sum_{\substack{1;k\\ 1;k>0}} \sum_{\substack{2;k\\ 0\leq 2;k<1;k}} \mathcal{V}^{NB}(|\mathbf{r}_{1;k} - \mathbf{r}_{2;k,m}|) + \sum_{\substack{j,\text{ parent chains}\\ j<k}} \sum_{\substack{1;k\\ 1;k\geq 0}} \sum_{\substack{2;j\\ 2;j\geq 0}} \mathcal{V}^{NB}(|\mathbf{r}_{1;k} - \mathbf{r}_{2;j,m}|)\} \tag{C.1}$$

$\mathcal{V}_\varphi$ is an intrinsic torsional potential associated with skeletal bonds, $\mathcal{V}^W$ is the potential exerted by the walls, and the last two terms correspond to self-chain and cross-chain nonbonded van der Waals interactions, respectively. $\mathbf{r}_{2;j,m}$ stands for the position of that image of atom $2;j$ that lies closest to $1;k$. The first derivatives of $\mathcal{V}(\mathbf{r}_0,\phi,\psi)$ with respect to all microscopic degrees of freedom are required for the minimization algorithm; they are found by direct differentiation and implementation of the chain rule. For the calculation of self-chain contributions to the gradient, eqs A.9 and A.10 of ref 8 are directly applicable. When atoms $1;k$ and $2;j$ correspond to different parent chains ($k \neq j$), $\partial|\mathbf{r}_{1;k} - \mathbf{r}_{2;j,m}|/\partial\psi_{i;k}$ and $\partial|\mathbf{r}_{1;k} - \mathbf{r}_{2;j,m}|/\partial\phi_{i;k}$ are determined via eqs A.9 and A.10b of ref 8 by substituting index 1 with $1;k$, index 2 with $2;j$, and index i with $i;k$.

The start coordinates $\mathbf{r}_{0;1}$ of the first chain are defined with respect to the box frame of reference. Chain start coordinates $\mathbf{r}_{0;k}$ of subsequent chains are defined relative to the first one. A displacement of the first chain start will not change any of the atom–atom separations; however, it will change all atom–wall distances when walls are implemented. Thus, none of the coordinates $x_{0;1}$, $y_{0;1}$, $z_{0;1}$ is a degree of freedom in the absence of walls (stage iii of the minimization). On the contrary, $z_{0;1}$ does become a degree of freedom when the wall potential is active (stages i and ii of the minimization). The derivatives $\partial\mathbf{r}_{1;k}/\partial\mathbf{r}_{0;1}$ and $\partial|\mathbf{r}_{1;k} - \mathbf{r}_{2;j,m}|/\partial\mathbf{r}_{0;k}$ are calculated straightforwardly; they can only assume the values of one or zero.

Appendix D. An Alternative Thermodynamic Analysis of Surface Area Changes of the Glassy Film

In section 4 and Appendix A we treated the entire glassy polymer film, including its anisotropic surface region, as a single phase. An alternative formulation, used frequently in the macroscopic treatment of surface phenomena,

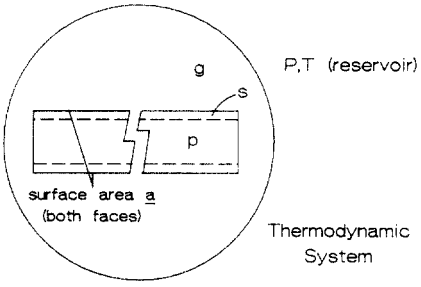

Figure 15. Phases involved in the thermodynamic analysis of Appendix D.

distinguishes a separate surface phase. Surface tension is defined in terms of this surface phase. A particularly lucid exposition of this formulation is given by Modell and Reid (ref 25, Chapter 13). Here, we briefly apply this alternative approach to our glassy film and discuss the insights it provides about eq 7.

Consider a one-component, closed thermodynamic system, consisting of our planar glassy polymer film at equilibrium with its own vapor (Figure 15). We distinguish three phases in the system: the bulk polymer phase p in the central region of the film, the vapor phase g, and the surface phase s. Phases p and g are isotropic, while phase s, whose definition is only possible with some degree of arbitrariness,[25] is anisotropic. Phase g surrounds phase p completely and is in contact with a temperature and pressure reservoir (which can be conceived of as being just more vapor). The pressure of the reservoir is, of course, extremely low, due to the involatility of the polymer. The thickness of the film is small relative to its lateral dimensions, and edge effects are neglected. We will assume that the glassy film is in a metastable thermodynamic state, as a result of which it cannot change shape (i.e., turn into a sphere); its thermodynamics is formulated around this state.

The equilibrium conditions for such a thermodynamic system are developed in ref 25. Phases p, g, and s have the same temperature and chemical potential. Under the planar geometry of interest here, the (normal) pressure is the same across all phases. The fundamental equations for each phase, in the energy representation, are

$$\mathrm{d}\underline{U}^{\mathrm{g}} = T\,\mathrm{d}\underline{S}^{\mathrm{g}} - P\,\mathrm{d}\underline{V}^{\mathrm{g}} + \mu\,\mathrm{d}n^{\mathrm{g}} \tag{D.1}$$

$$\mathrm{d}\underline{U}^{\mathrm{p}} = T\,\mathrm{d}\underline{S}^{\mathrm{p}} - P\,\mathrm{d}\underline{V}^{\mathrm{p}} + \mu\,\mathrm{d}n^{\mathrm{p}} \tag{D.2}$$

$$\mathrm{d}\underline{U}^{\mathrm{s}} = T\,\mathrm{d}\underline{S}^{\mathrm{s}} - P\,\mathrm{d}\underline{V}^{\mathrm{s}} + \mu\,\mathrm{d}n^{\mathrm{s}} + \gamma\,\mathrm{d}\underline{a} \tag{D.3}$$

Equation D.3 serves as a definition for surface tension.

We are interested in the quantity $\gamma - T\,\mathrm{d}\gamma/\mathrm{d}T$, where the temperature derivative is evaluated while the system p + g + s remains at (metastable) equilibrium. Straightforward thermodynamic analysis[25] leads to the exact result:

$$\gamma - T\frac{\mathrm{d}\gamma}{\mathrm{d}T} = \left(\frac{\underline{U}^{\mathrm{s}}}{\underline{a}} - \frac{n^{\mathrm{s}}}{\underline{a}}U^{\mathrm{p}}\right) - \frac{U^{\mathrm{g}} - U^{\mathrm{p}}}{V^{\mathrm{g}} - V^{\mathrm{p}}}\left(\frac{\underline{V}^{\mathrm{s}}}{\underline{a}} - \frac{n^{\mathrm{s}}}{\underline{a}}V^{\mathrm{p}}\right) = \left(\frac{\underline{H}^{\mathrm{s}}}{\underline{a}} - \frac{n^{\mathrm{s}}}{\underline{a}}H^{\mathrm{p}}\right) - \frac{H^{\mathrm{g}} - H^{\mathrm{p}}}{V^{\mathrm{g}} - V^{\mathrm{p}}}\left(\frac{\underline{V}^{\mathrm{s}}}{\underline{a}} - \frac{n^{\mathrm{s}}}{\underline{a}}V^{\mathrm{p}}\right) \tag{D.4}$$

One can show that eq D.4 is invariant with respect to the choice of a thickness for the surface phase s.

If one chooses phase s so as to exclude any appreciable amount of vapor phase from it, $\underline{V}^{\mathrm{s}}/n^{\mathrm{s}}$ is comparable in magnitude to V^{p}. Also, $U^{\mathrm{g}} - U^{\mathrm{p}}$ (energy of sublimation of the film) is a bounded quantity. On the contrary, at the very low pressures of interest here, the molar volume V^{g} is very large and causes the second term of eq D.4 to become negligible relative to the first one.[25] In other words, to an excellent approximation

$$\gamma - T\frac{\mathrm{d}\gamma}{\mathrm{d}T} = \frac{\underline{U}^{\mathrm{s}}}{\underline{a}} - \frac{n^{\mathrm{s}}}{\underline{a}}U^{\mathrm{p}} \tag{D.5}$$

Consider now the derivative

$$\left.\frac{\mathrm{d}\underline{U}}{\mathrm{d}\underline{a}}\right|_{n,T} \equiv \left.\frac{\mathrm{d}(\underline{U}^{\mathrm{p}} + \underline{U}^{\mathrm{s}})}{\mathrm{d}\underline{a}}\right|_{n^{\mathrm{p}}+n^{\mathrm{s}},T} \tag{D.6}$$

This derivative is evaluated under conditions such that phases p, g, and s are at equilibrium. Straightforward algebraic manipulations of eqs D.5 and D.6 give

$$\left.\frac{\mathrm{d}\underline{U}}{\mathrm{d}\underline{a}}\right|_{n,T} - \left(\gamma - T\frac{\mathrm{d}\gamma}{\mathrm{d}T}\right) = \underline{a}\frac{\mathrm{d}}{\mathrm{d}\underline{a}}\left(\frac{\underline{U}^{\mathrm{s}}}{\underline{a}} - \frac{n^{\mathrm{s}}}{\underline{a}}\right)\Bigg|_{n^{\mathrm{p}}+n^{\mathrm{s}},T} + (n^{\mathrm{p}} + n^{\mathrm{s}})\left.\frac{\mathrm{d}U^{\mathrm{p}}}{\mathrm{d}\underline{a}}\right|_{n^{\mathrm{p}}+n^{\mathrm{s}},T} = \underline{a}\frac{\mathrm{d}}{\mathrm{d}\underline{a}}\left(\gamma - T\frac{\mathrm{d}\gamma}{\mathrm{d}T}\right)\Bigg|_{n^{\mathrm{p}}+n^{\mathrm{s}},T} + (n^{\mathrm{p}} + n^{\mathrm{s}})\left.\frac{\mathrm{d}U^{\mathrm{p}}}{\mathrm{d}\underline{a}}\right|_{n^{\mathrm{p}}+n^{\mathrm{s}},T} \tag{D.7}$$

For a thick enough film, the quantities $\gamma - T\,\mathrm{d}\gamma/\mathrm{d}T$ and U^{p} at equilibrium should be intensive properties, independent of $\underline{a}$ and $n^{\mathrm{p}} + n^{\mathrm{s}}$. Thus, we conclude that $\mathrm{d}\underline{U}/\mathrm{d}\underline{a}|_{n,T}$ provides an excellent estimate of the measurable quantity $\gamma - T\,\mathrm{d}\gamma/\mathrm{d}T$.

In view of the statistical mechanical analysis of Appendix A, the quantity $\mathrm{d}\underline{U}/\mathrm{d}\underline{a}|_{n,T}$ can be estimated as follows: Take a model glassy microstate; modify its periodic boundaries in the x and y directions so that its surface area increases by $\Delta\underline{a}$; relax anew, under the modified boundary conditions; calculate the change $\Delta\mathcal{V}^0$ in total potential energy before and after the area change; finally, calculate the finite difference ratio $\Delta\mathcal{V}^0/\Delta\underline{a}$.

In practice, it was found that a volume-preserving affine deformation on the model film yields an estimate of $\mathrm{d}\mathcal{V}^0/\mathrm{d}\underline{a}$ that is indistinguishable from $\Delta\mathcal{V}^0/\Delta\underline{a}$ within the error of our calculation (see also ref 8). The affine deformation route (Appendix E) was thus chosen for the production phase of our work, due to its computational efficiency.

Appendix E. Derivation of the Internal Energy Contribution to Surface Tension for a Bonded System

Consider a system of atoms which can interact with each other via pairwise nonbonded (central) and bonded (not necessarily central) forces. In addition, there are torques associated with rotation around some bonds. We focus on an *infinitesimal affine* deformation of such a system, whereby all atomic coordinates are transformed according to the linear rule:

$$\mathbf{r}_i^{\,\mathrm{affine}} = \mathbf{A}\mathbf{r}_i + \mathbf{b} \tag{E.1}$$

The deformation is characterized by a strain tensor

$$\epsilon = {}^1/_2(\mathbf{A}^{\mathrm{T}}\mathbf{A} - \mathbf{I}) \approx {}^1/_2(\mathbf{A}^{\mathrm{T}} + \mathbf{A}) - \mathbf{I} \qquad (\epsilon_{LM} \ll 1) \tag{E.2}$$

The reversible work done by the system during this deformation has been shown[10] to be

$$\mathrm{d}W = \sum_L\sum_M\sum_i\Big\{\sum_{j\neq i}(1/2)[(r_{i,L} - r_{j,L})F_{ij,M} + \sum_K \mathbf{e}_{LMK}((T^{\mathrm{B}}{}_{ij,K} + T^{\mathrm{B}}{}_{ji,K})/2)]\Big\}\epsilon_{LM} \tag{E.3}$$

In eq E.3, $\mathbf{F}_{ij}$ stands for the total (bonded and nonbonded) force on atom i due to atom j; $\mathbf{T}^{B}_{ij}$ is the bonded torque on atom i due to atom j; $\mathbf{e}_{LMK}$ is the alternating tensor; and L, M, and K symbolize the three coordinate directions x, y, and z. Equation E.3 is applicable to each of our model film microstructures. For a volume-preserving deformation that leaves the direction of axes x, y, and z unchanged, the strain tensor ϵ_{LM} has the following diagonal form:

$$\epsilon = \begin{vmatrix} \epsilon_1 & 0 & 0 \\ 0 & \epsilon_2 & 0 \\ 0 & 0 & \epsilon_3 \end{vmatrix} \tag{E.4}$$

$$\epsilon_1 + \epsilon_2 + \epsilon_3 = 0 \tag{E.5}$$

Combining eqs E.3–E.5 and realizing that the torque contribution drops out for the deformation considered here, we simplify the total work to

$$\mathrm{d}W = \frac{1}{2}\sum_i \sum_{j\neq i} \{\epsilon_1(x_i - x_j)F_{ij,x} + \epsilon_2(y_i - y_j)F_{ij,y} - (\epsilon_1 + \epsilon_2)(z_i - z_j)F_{ij,z}\} \tag{E.6}$$

The change in total (upper and lower) surface area accompanying this infinitesimal affine deformation is

$$\mathrm{d}\underline{a} = \underline{a}_{\text{affine}} - \underline{a}_{\text{undeformed}} = \underline{a}(\epsilon_1 + \epsilon_2) \tag{E.7}$$

The change in total potential energy, $\mathrm{d}\mathcal{V}$, associated with the imposed differential deformation is equal to $-\mathrm{d}W$. On the other hand (see Appendices A and D), under isothermal conditions, $\mathrm{d}\mathcal{V}$ provides a good estimate of the internal energy change $\mathrm{d}\underline{U}$ of the microstructure. Therefore, from eqs E.6 and E.7

$$\left.\mathrm{d}\underline{U}\right|_{T,V,n} = -\frac{\mathrm{d}\underline{a}}{2\underline{a}}\sum_i \sum_{j\neq i}\left\{\frac{\epsilon_1}{\epsilon_1 + \epsilon_2}(x_i - x_j)F_{ij,x} + \frac{\epsilon_2}{\epsilon_1 + \epsilon_2}(y_i - y_j)F_{ij,y} - (z_i - z_j)F_{ij,z}\right\} \tag{E.8}$$

Taking $\epsilon_1 = \epsilon_2$ and realizing that interactions in our model system are accounted explicitly only between nearest-neighbor images, we obtain

$$\left.\frac{\mathrm{d}\underline{U}}{\mathrm{d}\underline{a}}\right|_{T,V,n} = -\frac{1}{2\underline{a}}\sum_i \sum_{j\neq i}\left\{\frac{1}{2}(x_i - x_j)_{\min}F^{\min}_{ij,x} + \frac{1}{2}(y_i - y_j)_{\min}F^{\min}_{ij,y} - (z_i - z_j)F^{\min}_{ij,z}\right\} \tag{E.9}$$

In eq E.9, $\underline{a}$ is taken as the total surface area (top and bottom) of one image of the model box and the summation takes place over this primary image. Equation 8 follows from E.9 by averaging over all model microstates and using eq 7.

In refs 9 and 10, methods for calculating the atomic-level stress tensors σ_i and the internal stress tensor σ in a bulk model system were presented. Our model films are intrinsically anisotropic. Over small sections Δz of the films, one can define a local internal stress tensor $\sigma(z)$, whose transverse component depends on position. This definition of internal stress follows that of Harasima.[34] By virtue of eq 8 and using the notation of ref 10, γ^U can be expressed as

$$\gamma^U = \frac{1}{\underline{a}}\left\langle \sum_{i \text{ atoms in box}} [(\sigma_{i,xx} + \sigma_{i,yy})/2 - \sigma_{i,zz}]V_i \right\rangle \tag{E.10}$$

In eq E.10, V_i is the "atomic volume" used in the definition of the atomic stress tensor.[9] Passing to a continuum description, where σ is solely a function of z

$$\gamma^U = \frac{1}{\underline{a}}\left\langle \sum_{k \text{ all sections of film}} [(\sigma_{xx,k} + \sigma_{yy,k})/2 - \sigma_{zz,k}]\Delta V_k \right\rangle = \frac{1}{2}\left\langle \sum_{k \text{ all sections of film}} [(\sigma_{xx,k} + \sigma_{yy,k})/2 - \sigma_{zz,k}]\Delta z_k \right\rangle \tag{E.11}$$

Equation E.11 is entirely analogous to the "mechanical definition" of surface tension.[35] By plotting the distributions of σ_{xx}, σ_{yy}, and σ_{zz} across the film, including tail corrections (Appendix G), it was established that all diagonal components of the internal stress are equal in the middle region, as expected of a bulk polymer phase. Thus, all contributions to γ^U in eq E.11 come from two roughly 20-Å-thick regions near the free surfaces.

Appendix F. Alternative Expression for γ^U in Terms of Interchain Nonbonded Forces Only

Equation 8 and its analogue for the internal stress tensor (eq 65 of ref 9) require knowledge of the bonded forces between atoms. It is possible, however, to calculate σ and γ^U based on nonbonded forces only.

Starting from eq 63 of ref 9 and making use of the periodicity of the model system, the reciprocity of interatomic interactions, and the conditions of detailed mechanical equilibrium, one can arrive at the following equivalent expression for the internal stress tensor:

$$\sigma_{LM} = \frac{1}{\underline{V}}\sum_{i \text{ in box}} r^{P}_{i,L}\Big\{\sum_{\substack{j \text{ in box} \\ i,j_{\min}(i) \text{ belong to different images of same parent chain or, correspond to different parent chains}}} F^{\mathrm{NB,min}}_{ij,M}\Big\} - \frac{1}{2\underline{V}}\sum_{i \text{ in box}}\sum_{j \text{ in box}} (r_{i,L} - r_{j,L})_{\min}F^{\mathrm{NB,min}}_{ij,M} \tag{F.1}$$

($i,j_{\min}(i)$ belong to different images of same parent chain or correspond to different parent chains)

In eq F.1, $\mathbf{r}^{P}_i$ stands for the position of the parent chain image of atom i. Equation F.1 is invariant to which particular image of a chain is selected as the parent chain. Note that the summations extend over *all interchain contributions*, i.e., over all interacting pairs of atoms except those belonging to the same image of the same parent chain.

A corresponding expression is readily derived for γ^U:

$$\gamma^U = \frac{1}{\underline{a}}\left\langle \sum_{i \text{ in box}}\sum_{j \text{ in box}} \left\{\left(\frac{1}{2}x^{P}_{i}F^{\mathrm{NB,min}}_{ij,x} + \frac{1}{2}y^{P}_{i}F^{\mathrm{NB,min}}_{ij,y} - z^{P}_{i}F^{\mathrm{NB,min}}_{ij,z}\right) - \frac{1}{2}\left[\frac{1}{2}(x_i - x_j)_{\min}F^{\mathrm{NB,min}}_{ij,x} + \frac{1}{2}(y_i - y_j)_{\min}F^{\mathrm{NB,min}}_{ij,y} - (z_i - z_j)F^{\mathrm{NB,min}}_{ij,z}\right]\right\}\right\rangle \tag{F.2}$$

($i,j_{\min}(i)$ belong to different images of same parent chain or correspond to different parent chains)

A great advantage of eqs F.1 and F.2 over the equations we have derived previously is that the new equations are applicable even to microstates not satisfying the conditions of detailed mechanical equilibrium. In such microstates, the forces associated with the bond length and bond angle constraints are indeterminate, unless the atomic momenta are also known. On the contrary, the right-hand sides of eqs F.1 and F.2 can readily be evaluated from configuration alone. Thus, the new equations are usable for computing the pressure tensor and the surface tension from Monte Carlo simulations of multichain systems with realistically constrained geometries. A general derivation of these equations will be presented elsewhere. Application of eqs 8 and F.2 to our model microstates leads to identical estimates for γ^U, as expected.

From eqs F.1 and F.2, it is obvious that the values of σ and γ^U are shaped by interchain interactions. The error in theoretical estimates of these quantities should thus decrease roughly in inverse proportion to the square root of the number of chains in the model system. This explains the large error with which these quantities are estimated in this work (compare eq 9).

Appendix G. Derivation of the Long-Range Contribution to γ^U

The summations involved in the formulas for the internal energy contribution to surface tension (eqs 8 and F.2) are taken over minimum image pairs of atoms. Only minimum image pairs interact explicitly via the finite range potential we use for creating our model films. Long-range attractions due to the omitted potential tails, however, have a serious effect on thermodynamic properties, such as the surface tension.[12] For a correct estimation of γ^U we must include the contribution of tails a posteriori, taking into account the nonuniform density profile of the film. A brief description of how this is accomplished follows.

Consider two atoms in the model box, i and j. We wish to calculate the contribution to γ^U due to interactions between i and all images of j that have not been included explicitly in the summation of eq 8. To do this, we "smear" atom j and its period images into a slice of infinitesimal thickness δ and atomic density $2/\underline{a}\delta$ parallel to the xy plane. Note that with this choice of density, there is exactly one image of j per model box.

Let

$$K^{\text{tails}}{}_{LM,ij}(r_1,r_2) = \sum_{\substack{j',\text{ all images}\\ \text{of } j \text{ within}\\ \text{distance } r_1\\ \text{to } r_2 \text{ from } i}} (r_{i,L} - r_{j',L})(F^{\text{LJ}}{}_{ij',M} - F^{\text{NB}}{}_{ij',M}) \tag{G.1}$$

where r_1 and r_2 are two distances such that $r_2 > r_1$ and $r_2 > |z_j - z_i|$. In eq G.1, $\mathbf{F}^{\text{LJ}}{}_{ij}$ and $\mathbf{F}^{\text{NB}}{}_{ij}$ stand for the force of interaction calculated according to the full Lennard-Jones ($\mathcal{V}^{\text{LJ}}{}_{ij}$) and according to the finite-range nonbonded interaction potential ($\mathcal{V}^{\text{NB}}{}_{ij}$), respectively.[8]

In our smeared representation of j, the above tail contribution is approximated by the following integral (see Figure 16):

$$K^{\text{tails}}{}_{LM,ij} = \int_{z_j}^{z_j+\delta} dz \int_{\rho_1}^{\rho_2} \rho\, d\rho \int_0^{2\pi} d\phi\, (2/\underline{a}\delta) f'_{ij}\{[\rho^2 + (z_j - z_i)^2]^{1/2}\} \frac{(r_{i,L} - r_{j,L})(r_{j,M} - r_{i,M})}{[\rho^2 + (z_j - z_i)^2]^{1/2}} \tag{G.2}$$

where ρ is the radial distance of the smeared images of j from the projection of i on their plane, $\rho_1 = \{\max([r_1^2 - (z_j - z_i)^2], 0)\}^{1/2}$, $\rho_2 = \{\max([r_2^2 - (z_j - z_i)^2], 0)\}^{1/2}$, $f_{ij}(r) = \mathcal{V}^{\text{LJ}}{}_{ij}(r) - \mathcal{V}^{\text{NB}}{}_{ij}(r)$, and

$$f'_{ij}(r) = df_{ij}(r)/dr \tag{G.3}$$

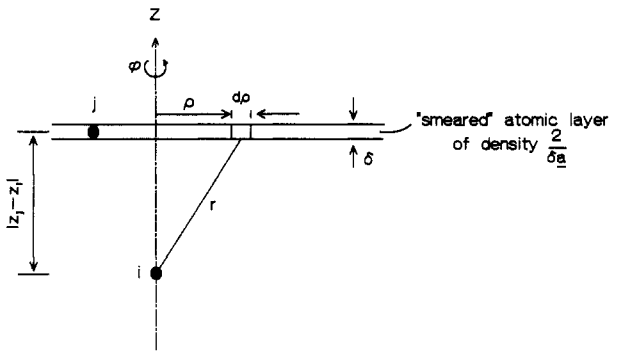

Figure 16. Pictorial representation of the two-dimensional "smearing" approximation used for calculating the tail contribution to γ^U from a pair of atoms (i, j) in the primary box. The notation of eq G.2 is explained.

Equation G.2 can by analytically integrated for each atom pair (i, j). Calculations reveal that all off-diagonal terms of the form $K^{\text{tails}}{}_{LM,ij}(r_1,r_2)$ with $L \neq M$ are identically zero. The remaining significant terms are

$$K^{\text{tails}}{}_{xx,ij}(r_1,r_2) = K^{\text{tails}}{}_{yy,ij}(r_1,r_2) = -\frac{2\pi}{\underline{a}}\{[r_2^2 - (z_j - z_i)^2] f_{ij}(r_2) - \max([r_1^2 - (z_j - z_i)^2], 0)\, f_{ij}[\max(r_1, |z_j - z_i|)]\} + \frac{4\pi}{\underline{a}} \int_{\max(r_1,|z_j-z_i|)}^{r_2} r f_{ij}(r)\, dr \tag{G.4}$$

$$K^{\text{tails}}{}_{zz,ij}(r_1,r_2) = -\frac{4\pi}{\underline{a}}(z_i - z_j)^2\{f_{ij}(r_2) - f_{ij}[\max(r_1, |z_j - z_i|)]\} \tag{G.5}$$

In evaluating the right-hand side of eqs G.4 and G.5, it is useful to break up the r domain into two parts: one ($R_{1,ij}$ to R_{ij}) in which $\mathcal{V}^{\text{NB}}{}_{ij}$ is given by a quintic spline function of interatomc distance,[8] and one (R_{ij} to ∞) in which $\mathcal{V}^{\text{NB}}{}_{ij}$ is zero.

Thus, the correction for γ^U due to tails (compare eqs E.9 and G.1) is

$$\gamma^U{}_{\text{tails}} = -\frac{1}{2\underline{a}} \sum_i \sum_{j \neq i} \left\{ \frac{1}{2}[K^{\text{tails}}{}_{xx,ij}(r_1 = R_{1,ij}; r_2 = R_{ij}) + K^{\text{tails}}{}_{xx,ij}(r_1 = R_{ij}; r_2 \to \infty) + K^{\text{tails}}{}_{yy,ij}(r_1 = R_{1,ij}; r_2 = R_{ij}) + K^{\text{tails}}{}_{yy,ij}(r_1 = R_{ij}; r_2 \to \infty)] - [K^{\text{tails}}{}_{zz,ij}(r_1 = R_{1,ij}; r_2 = R_{ij}) + K^{\text{tails}}{}_{zz,ij}(r_1 = R_{ij}; r_2 \to \infty)] \right\} \tag{G.6}$$

with $K^{\text{tails}}{}_{xx}$, $K^{\text{tails}}{}_{yy}$, and $K^{\text{tails}}{}_{zz}$ calculated from eqs G.4 and G.5. Note that the summation in eq G.6 takes place over all pairs of atoms in the unit cell, including those that are bonded.

The average tail contribution calculated in this way from our 70 static microstructures was

$$\gamma^U{}_{\text{tails}} = 22.5 \pm 0.5 \text{ mN/m} \tag{G.7}$$

Comparison with the total estimate for γ^U (eq 9) shows that $\gamma^U{}_{\text{tails}}$ amounts to 52% of γ^U and is therefore far from negligible.

References and Notes

(1) Madden, W. G. *J. Chem. Phys.* **1987**, *87*, 1405.
(2) Lastoskie, C.; Madden, W. G. *Polym. Prepr. (Am. Chem. Soc., Div. Polym. Chem.)* **1989**, *30* (2), 39.

(3) ten Brinke, G.; Ausserré, D.; Hadzioannou, G. *J. Chem. Phys.* **1988**, *89*, 4374.
(4) Mansfield, K. F.; Theodorou, D. N. *Macromolecules* **1989**, *22*, 3143.
(5) Kumar, S. K.; Vacatello, M.; Yoon, D. Y. *J. Chem. Phys.* **1988** *89*, 5206; *Macromolecules* **1990**, *23*, 2189.
(6) Yethiraj, A.; Hall, C. K. *J. Chem. Phys.* **1989**, *91*, 4827.
(7) Bitsanis, I.; Hadziioannou, G. *Polym. Prepr. (Am. Chem. Soc., Div. Polym. Chem.)* **1989**, *30* (2), 78.
(8) Theodorou, D. N.; Suter, U. W. *Macromolecules* **1985**, *18*, 1467.
(9) Theodorou, D. N.; Suter, U. W. *Macromolecules* **1986**, *19*, 139.
(10) Theodorou, D. N.; Suter, U. W. *Macromolecules* **1986**, *19*, 379.
(11) Theodorou, D. N.; Ludovice, P. J.; Suter, U. W. In *Scattering, Deformation, and Fracture in Polymers*; Wignall, G. D., et al., Eds.; Mater. Res. Soc. Symp. Proc. Vol. 79; Materials Research Society: Pittsburgh, 1987; pp 387–396.
(12) Allen, M. P.; Tildesley, D. J. *Computer Simulation of Liquids*; Clarendon Press: Oxford, 1987.
(13) Theodorou, D. N. *Macromolecules* **1989**, *22*, 4578.
(14) Bondi, A. *Physical Properties of Molecular Crystals, Liquids and Glasses*; Wiley: New York, 1968.
(15) Suter, U. W.; Flory, P. J. *Macromolecules* **1975**, *8*, 765.
(16) Flory, P. J. *Statistical Mechanics of Chain Molecules*; Interscience Publishers: New York, 1969.
(17) Flory, J. P. *Macromolecules* **1974**, *7*, 381.
(18) Hillstrom, K. *Nonlinear Optimization Routines in AMDLIB*, Technical Memorandum No. 297, Argonne National Laboratory, Applied Mathematics Division, Argonne, IL, 1976; Subroutine GQBFGS in AMDLIB.
(19) Teleman, O.; Jönsson, B. *J. Comput. Chem.* **1986**, *7*, 58.
(20) Abraham, F. F.; Schreiber, D. E.; Barker, J. A. *J. Chem. Phys.* **1975**, *62*, 1958. Chapela, G. A.; Saville, G.; Thompson, S. M.; Rowlinson, J. S. *J. Chem. Soc., Faraday Trans. 2* **1977**, *73*, 1133.
(21) Rubin, J. R.; Mazur, J. *Macromolecules* **1977**, *10*, 139.
(22) Theodorou, D. N.; Suter, U. W. *Macromolecules* **1985**, *18*, 1206.
(23) Wright, T. J. *Comput. Graphics* **1979**, *13*, 182; subroutine ISOSRF of the SCD Graphics System of the National Center for Atmospheric Research, Boulder, CO.
(24) Magda, J. J.; Tirrell, M. V.; Davis, H. T. *J. Chem. Phys.* **1985**, *83*, 1988.
(25) Modell, M.; Reid, R. C. *Thermodynamics and Its Applications*, 2nd ed.; Prentice-Hall: Englewood Cliffs, NJ, 1983.
(26) Swenson, R. J. *Am. J. Phys.* **1983**, *51*, 940.
(27) Thompson, S. M.; Gubbins, K. E. In *Computer Modeling of Matter*; Lykos, P., Ed.; ACS Symposium Series No. 86; American Chemical Society: Washington, DC, 1978; pp 76–85.
(28) Wu, S. *Polymer Interface and Adhesion*; Marcel Dekker: New York, 1982.
(29) Stillinger, F. H.; Weber, T. A. *Science* **1984**, *225*, 983. Weber, T. A.; Stillinger, F. H. *Phys. Rev. B* **1985**, *31*, 1954.
(30) Sylvester, M. F.; Yip, S.; Argon, A. S. *Polym. Prepr. (Am. Chem. Soc., Div. Polym. Chem.)* **1989**, *30* (2), 32.
(31) Weiner, J. H. *Statistical Mechanics of Elasticity*; Wiley: New York, 1983.
(32) Gō, N.; Scheraga, H. *Macromolecules* **1976**, *9*, 535.
(33) Honnell, K. G.; Hall, C. K.; Dickman, R. *J. Chem. Phys.* **1987**, *87*, 664.
(34) Walton, J. P. R. B.; Tildesley, D. J.; Rowlinson, J. S. *Mol. Phys.* **1983**, *48*, 1357.
(35) Evans, R. *Adv. Phys.* **1979**, *28*, 143.

Registry No. Atactic polypropylene, 9003-07-0.